Biotinylation of the flagellar hook in *E.coli*

Claudio Silvestrin

München 2010

Biotinylation of the flagellar hook in *E.coli*

Claudio Silvestrin

Diplomarbeit an der Fakultät für Physik

der Ludwig-Maximilians-Universität München

durchgeführt am Department of Physics

und Department of Biochemistry

der University of Oxford

vorgelegt von

Claudio Silvestrin

geboren in München

München, den 30. September 2010

Erstgutachter: Prof. Dr. Philip Tinnefeld

Zweitgutachter: Prof. Dr. Joachim Rädler

Abbreviations

Amp	Ampicillin
BAP	Biotin acceptor peptide
BSA	Bovine serum albumin
Cm	Chloramphenicol
DIC	Differential interference contrast
f/c	Final concentration
FW	Formula weight
IMF	Ion motive force
IPTG	Isopropyl β-D-1-thiogalactopyranoside
LB	Luria-Bertani-broth
MB	Motility buffer
PCR	Polymerase chain reaction
PMF	Proton motive force
SMF	Sodium motive force
TB	Tryptone-broth
w/v	Weight per volume

Contents

1 Abstract

The bacterial flagellar hook in *Escherichia coli* acts as a universal joint transmitting the rotation of the bacterial flagellar motor to the helical filament, which allows the bacterium to move about its environment. This study introduces genetically modified *E.coli* strains, carrying a tag in the hook-protein FlgE, which serves as a target for enzymatic biotinylation. Motility of the engineered strains is analysed followed by investigation of successful biotinylation by fluorescence microscopy. Two sites in FlgE were found which support the insertion of the 15-mer peptide and are biotinylated successfully. The strong streptavidin-biotin interaction is used in the biotinylated strains to attach streptavidin conjugated gold-beads to the flagellar hook, which allowed observation of stepping rotation of the bacterial flagellar motor. When exposed to free streptavidin, loss of motility could be observed in strains carrying the FlgE mutation. Bundle formation was analysed and compared to wildtype strains by visualisation of fluorescently labelled flagella in free swimming bacteria, which confirmed that streptavidin binding changes the elastic properties of the hook. The streptavidin-mediated change of the torsional compliance of bacterial hooks was quantified by tethering cells with locked motors to a glass surface by their flagella and measuring the rebound of the cells after being rotated and released with an optical tweezer. The engineered strains introduced in this study provided a tool for analysing and changing the elastic properties of the hook and for attachment of markers for analysis of the rotation of the bacterial flagellar motor.

2 Introduction

2.1 Bacterial propulsion

Many organisms rely on diffusion to obtain nutrients or transport excretions away. But this only allows them to survive in environments with high enough nutrient concentrations. An organism would benefit from being able to move about its environment if it can outrun diffusion [1]. This is why many bacteria developed systems to propel themselves through their surroundings towards favourable conditions, the term for which is Chemotaxis.

However the principles governing the interaction of microorganisms with their surroundings differ considerably from the laws of the macroscopic world, which we are used to through daily experience. In fluid mechanics liquid environments are characterised by the so called Reynolds-number, which quantifies the relative importance of inertial and viscous forces.

On the scale of microorganisms this number is small with the medium behaving like a viscous fluid without turbulent flow. At the same time microorganisms are exposed to strong fluctuations known as Brownian motion. Movement in these viscous and fluctuating environments has previously been described as "Swimming in molasses, walking in a hurricane. [2]", which suggests this is a quite challenging task for a single-celled organism. So how do they manage directional movement?

Several bacteria species like *Escherichia coli* or *Salmonella typhimurium* rotate helical flagellar filaments which drive the bacterium forward similar to marine propellers on a ship. The extraordinary machine driving this rotation is the bacterial flagellar motor, several copies of which (~5) are integrated in the bacterial membrane. The motor is powered by ion transfer through the cell membrane, which occurs due to the gradient of the electrochemical potential across the membrane maintained by the cell.
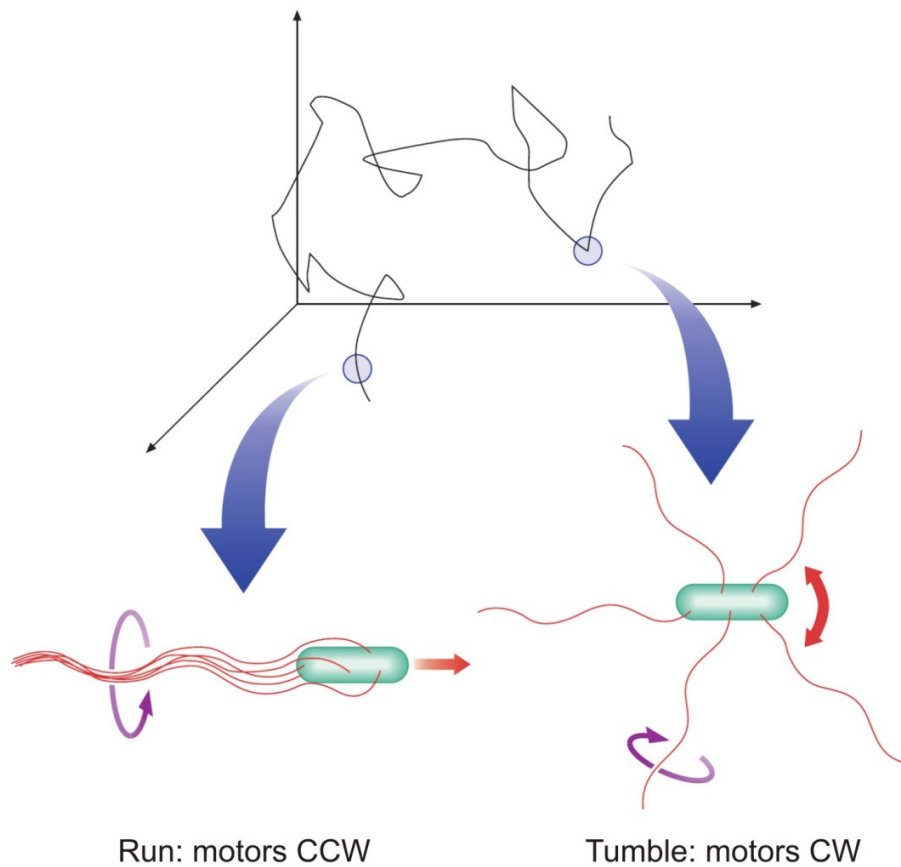
Run: motors CCW   Tumble: motors CW

Figure 1: *E.coli* swim by rotating their flagella. When rotated counter-clockwise (looking at the motor from outside the cell) the flagella synchronise and form a bundle, which acts as a propeller and allows the bacterium to move forward. To change its direction of movement towards more favourable conditions the bacterium changes the direction of rotation to clockwise whereupon the flagella fly apart resulting in a tumble, which reorients the cell randomly. These switching events are controlled by a chemotactic mechanism, which induces switching less frequently when the cell is swimming in a direction of increasing nutrient concentration. (Source: www.els.net)

Wildtype *E.coli* and *S.typhimurium* have stator units that are selective for protons, which means that the driving force is the proton motive force (PMF), however other species are driven by different ions e.g. Na^+ in *V.alginolyticus*.
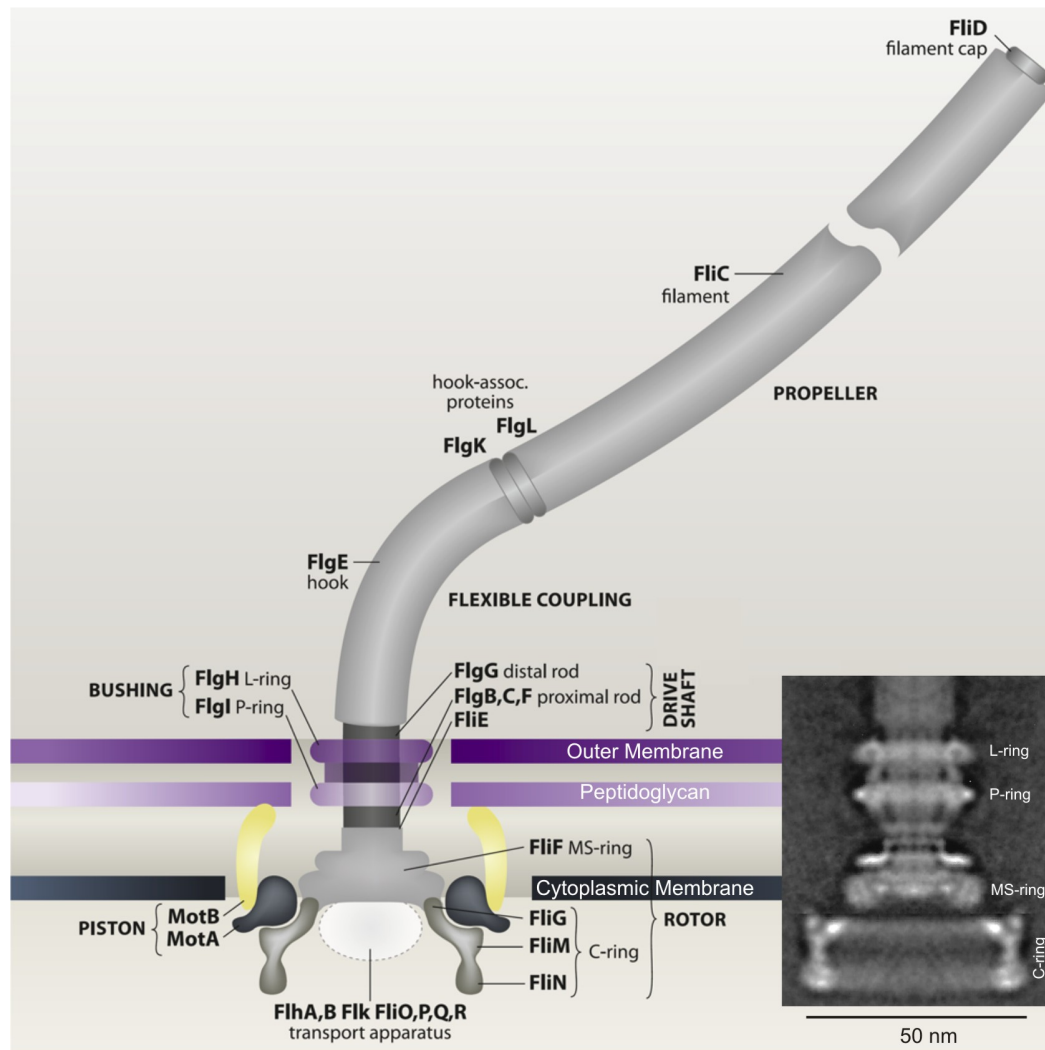
2.2 Bacterial flagellar motor

Figure 2: The bacterial flagellar motor. A schematic and an electron micrograph (inlet) are shown. (Sources: [3], [4])

The bacterial flagellar motor of *E.coli* contains 13 different types of proteins making up larger structures, which in turn constitute the building blocks for the motor. The similarity to man-made rotary motors is striking. The L- and the P-ring serve as a bushing for a structure resembling a motor shaft, the rod. Connected to it are two additional ring structures in the basal body, the MS and the C-ring, which make up the rotor. Several complexes made up of the proteins MotA and MotB have been identified as stator units. The interface between them and the FliG proteins in the rotating C-ring is believed to be the site of torque generation [5]. A remarkable property of the MotB stator units is that, instead of being a fixed unit in the motor, they have been found to diffuse in the membrane and exchange rapidly with the motor. Therefore this is, despite being

structurally similar to man-made motors, a highly dynamic biological structure which incorporates diffusion driven processes.

The structure is assembled in a specific order through guided self-assembly, see Figure 3 and Video 1 (supplementary material).
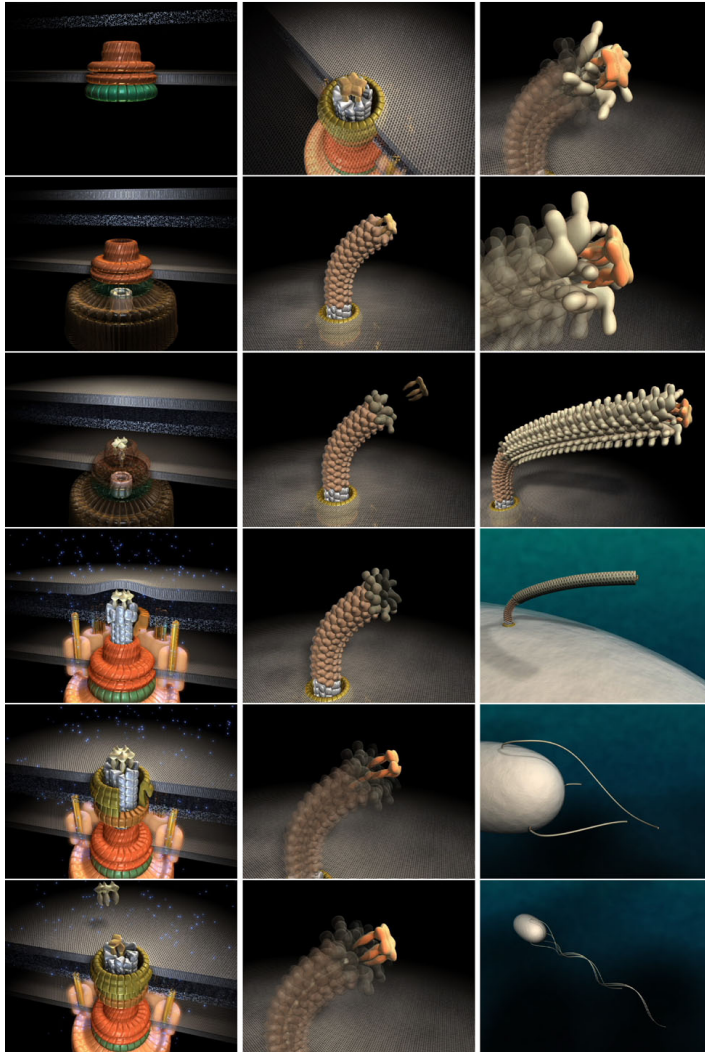

Figure 3: Assembly of the bacterial flagellar motor, the hook and the filament. The completion of the core structure is followed by assembly of the flagellum through an export apparatus. The individual proteins diffuse one-by-one through a channel inside the flagellum towards the tip where they are added to the structure. (Source: [6])

The flagellum consists of two main parts, the filament and the hook. The filament is a rigid helical structure which through rotation generates the force to propel the bacterium as described before.

2.3 Hook

At its basal end the filament is linked to the rotating rod of the motor by a flexible structure called the bacterial hook. It is frequently described as a universal joint, which allows the filament to rotate about a different axis to the motor, which is assumed to be necessary for bundle formation.

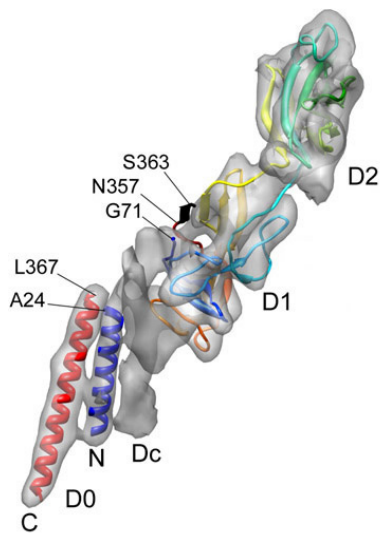The flagellar hook is a structure made up of ~120 copies of the protein FlgE, see Figure 4 and Figure 5.

Figure 4: The FlgE monomer or "hook-protein", the subunit of the hook, cut out from a density map. The four domains D0, Dc, D1, D2 are labelled. (Source: [7])
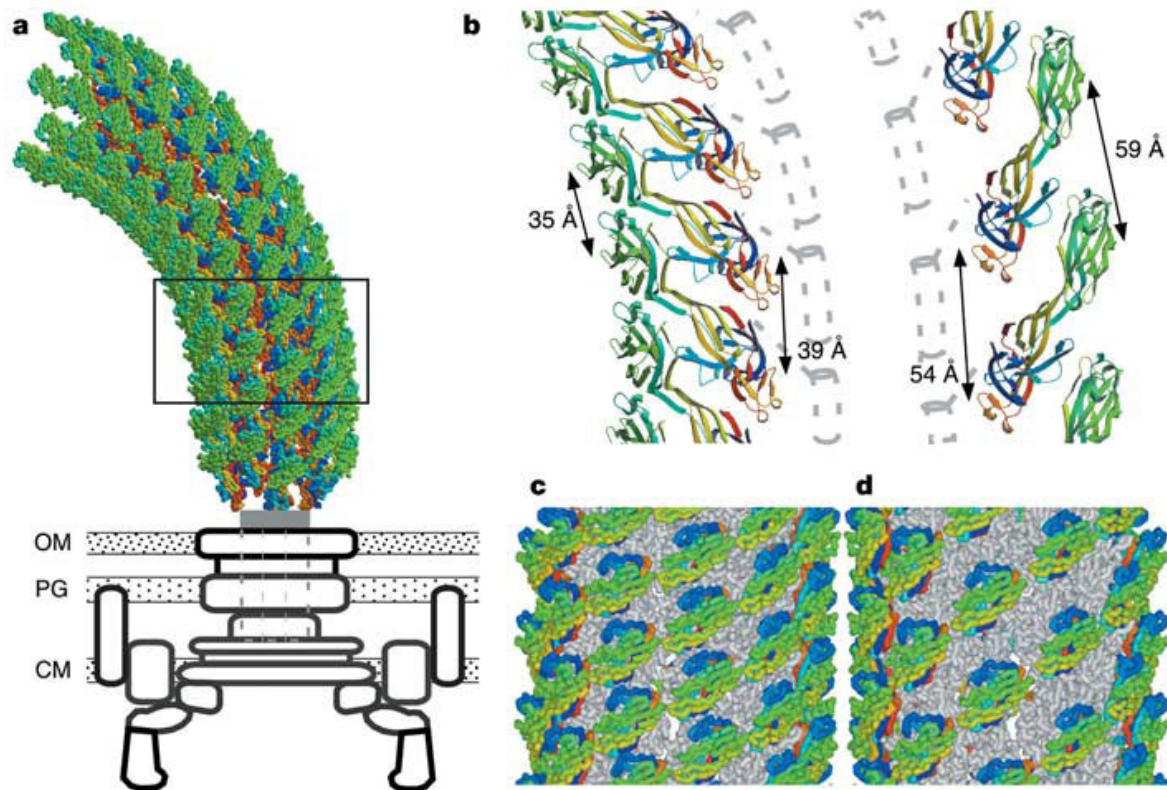
Figure 5: **a,** Atomic model of the coiled hook **b,** Magnified image of the coiled hook with the innermost and outermost protofilaments on the left and right, respectively. **c, d,** Intermolecular packing arrangements on the inner side (c) and on the outer side (d) of the coiled hook surface. Only domain D2 of FlgE is colour-coded; the inner domain D1 is coloured light grey. (Source: [8])

As evidenced by electron microscopy the hook is a highly curved structure [9]. Therefore protofilaments on the inside of the curve have a shorter repeat distance than those on the outside, see Figure 5. The structure undergoes continuous rolling rotation, during which the protofilaments dynamically change their conformation as well as their repeat distance [8].

To allow for the flagellar bundle to form all the filaments have to be rotated in phase. For this phase-matching the hook also has to accommodate a twist in its structure. Previous measurements have confirmed that the torsional compliance of the hook is greater than that of the filament [10].

16

2.4 Physics of bacterial propulsion

2.4.1 Swimming in molasses

As mentioned before the Reynolds number, which gives the ratio between the inertial and the viscous forces, is an important quantity to characterise the fluid dynamics on small scales.

$$\mathcal{R} = \frac{lv\rho}{\eta} \qquad (2.1)$$

where l is the characteristic length of the object (approximated as a sphere with radius l), v is the mean fluid velocity, ϱ is the density and η is the viscosity of the of the surrounding medium. The environments in which molecular motors have to produce work are dominated by viscous forces and therefore characterized by a low Reynolds number on the order of $\sim 10^{-4}$ (in comparison the movement of the smallest fish is characterised by a Reynolds number on the order of ~ 1). It might be sensible to ask why microorganisms like *E.coli* move in a manner so different from macroscopic swimming organisms like fish. The answer is that the equations of fluid mechanics become time reversible at low Reynolds numbers.
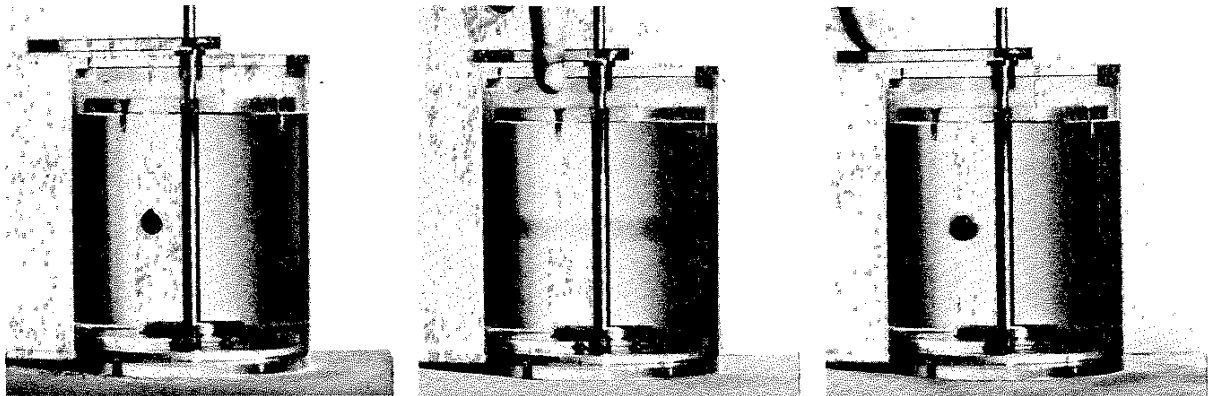

Figure 6: Time reversibility at low Reynolds numbers. A fluid element has been dyed in a viscous medium (left). The inner cylinder is then turned 4 times with the blob disappearing (centre). When turned back 4 times to the initial position the blob reappears. (Source: [11])

This means that reciprocal motion like a flapping fish tail generates no propulsion, because the movement generated by a stroke in one direction exactly cancels out the movement generated previously by the stroke in the other direction, thereby bringing the

organism back to its original position. However ciliates, a group of protozoans, can move by flapping their cilia back and forth. They key is that only the strokes going one way serve for propulsion, whereas for the reverse motion the cilium contracts, see Figure 7. This way the motion generated in the first stroke isn't cancelled out entirely and the ciliate makes net progress [12].

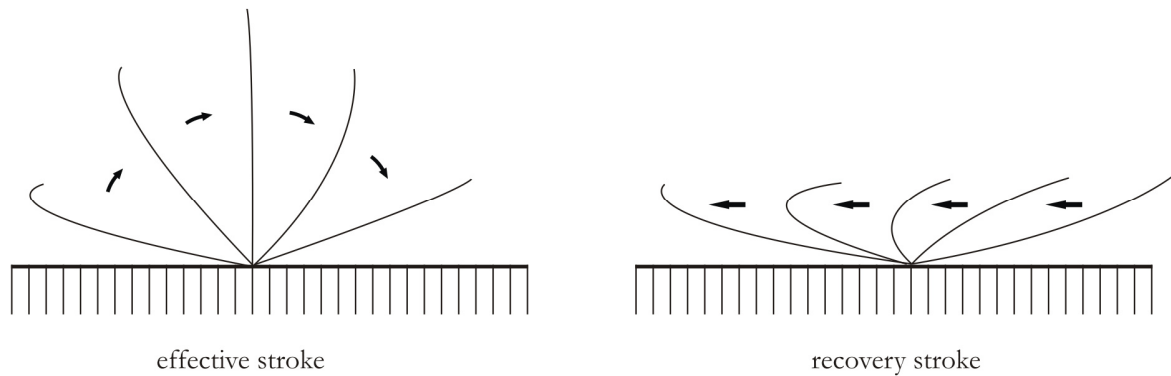effective stroke   recovery stroke

Figure 7: The ciliary cycle. The effective stroke (left) alternates with the recovery stroke (right). The motion is not reciprocal, so the cilium can make net progress in sweeping fluid past the surface.

The only way to avoid this partial cancellation while still effecting a non-reciprocal motion is by rotation. This is the reason why many bacteria move by rotating helical flagella. Some bacteria like *Rhodobacter sphaeroides* only use one flagellum for propulsion, but as mentioned before *E.coli* and *S.typhimurium* possess several flagella and need to synchronize them in a bundle. To analyse the mechanisms involved in bundle formation, Kim *et al.* used a macroscopic scale model of flagella driven by rotational motors in a viscous medium, choosing helix geometry and the Reynolds-number of the system to match the corresponding quantities of *E.coli*. They concluded that bundling is a purely mechanical phenomenon involving hydrodynamic interactions, bending and twisting elasticity, and geometry [13].
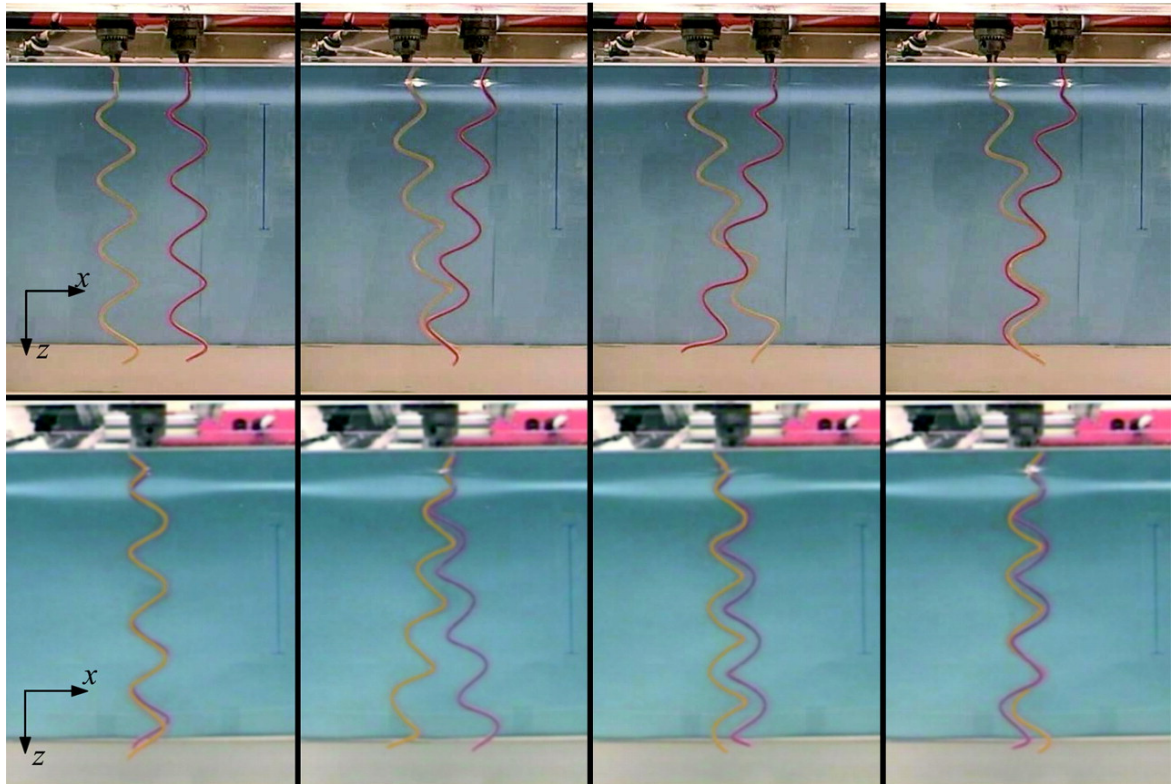
Figure 8: Macroscopic scale model of flagellar bundle formation shown at t = 0, 96, 168, 264 s. The lower sequence shows the helices from the side at the same times. The scale bars are 100 mm long; the helices are 310 mm long, 4.0 mm in diameter and turning at 0.1 Hz (Source: [13]).

2.4.2 Walking in a hurricane

The viscosity of their environment is not the only challenge for microorganisms. The working parts of molecular motors operate at energies comparable to the energy of the surrounding thermal bath. Thus thermal fluctuations have a profound effect on these motors. One way to generate motion is to bias these fluctuations by selectively stopping the fluctuations in one direction and letting through the ones in the other, comparable to a ratchet mechanism. This way the motor is able to do work against a load.
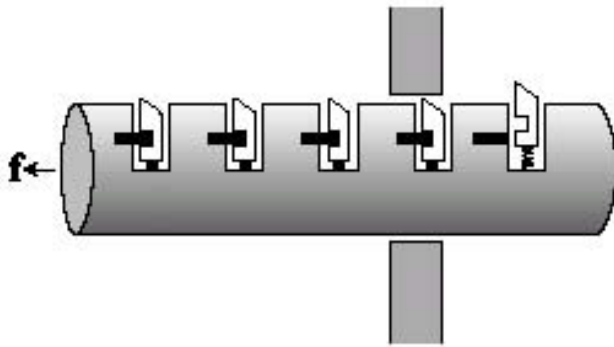
Figure 9: A ratchet in a thermal bath, channeling the fluctuations of the piston to do work against a load. The bolts are tied down on the left side, then released as they emerge on the right. (Source: [12])

Channeling the thermal fluctuations in such a way requires a free energy source, which motors like the well known kinesin obtain by ATP hydrolysis.

An example for motors operating like thermal ratchets is kinesin, which transports cargoes in cells by walking along the microtubule cytoskeleton with its two heads, see Figure 10. Here the binding of ATP results in a conformational change of the neck linker of the bound head. This moves the fluctuating unbound head forward, making it more likely to bind to the microtubules element in front of it, resulting in forward stepping.
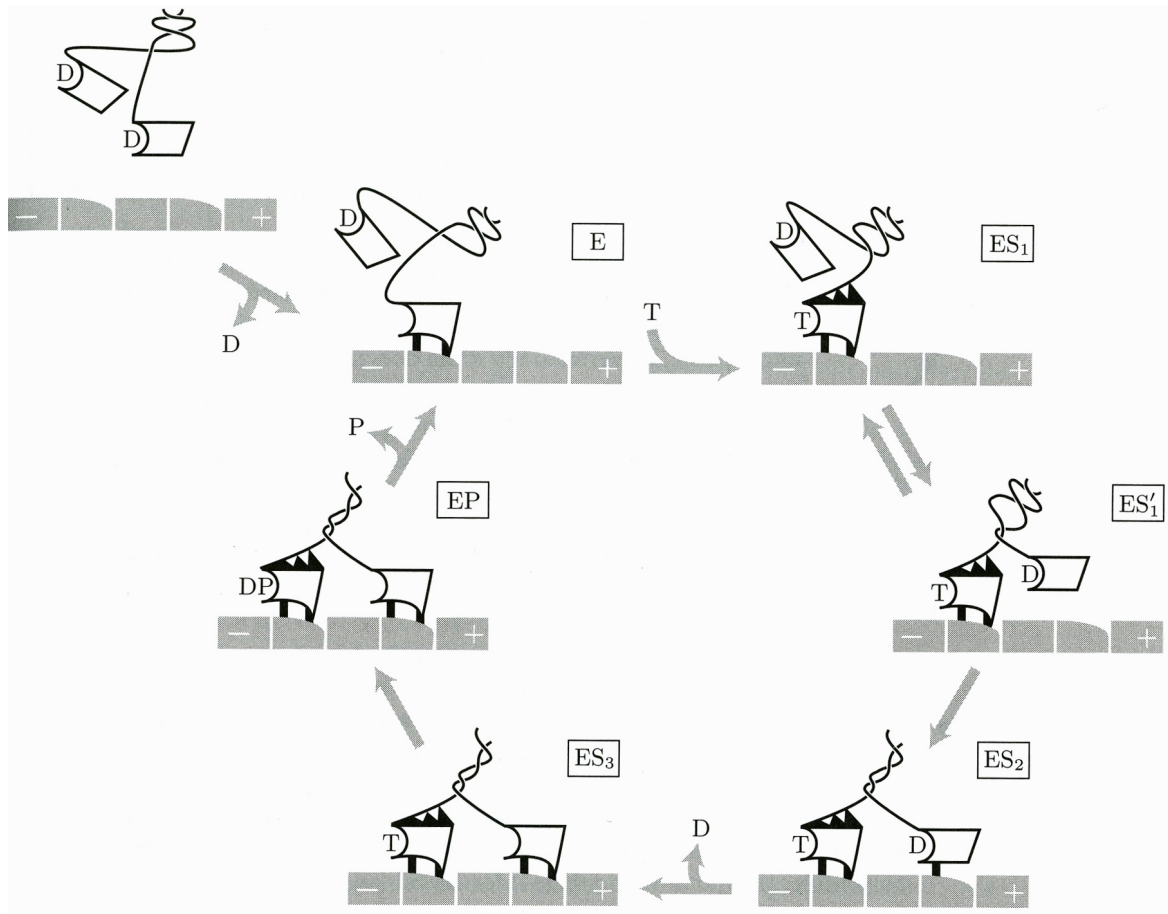
Figure 10: Model for kinesin stepping. Each kinesin head has a binding site for the microtubule and a second binding site for a nucleotide such as ATP. The heads are connected to the α-helical coiled coil by a flexible 15-mer chain called the neck linker. The microtubules are shown in grey with their "+" end at the right. Two black lines represent strong physical bonds, whereas single lines represent a weak bond. The symbols T, D, and P are short for ATP, ADP and inorganic phosphate, respectively. The states are labelled by E (Enzyme), ES (Enzyme-Substrate Complex) and EP (Enzyme-Product Complex). Binding of ATP to the bound kinesin head in the state ES_1 results in a conformational change of its neck linker, biasing the other head's random motion in the forward direction. (Source: [12])

Other molecular motors like myosin are believed to be working with a power-stroke mechanism. Here the chemical transition leads to a conformational change that pulls the motor protein forward rather than just biasing fluctuations.

2.4.3 Free Energy

When in contact with a thermal bath interactions with the surroundings have to be considered. A driven process not only uses up the available energy but also increases the entropy. To take this into account we need to look at the change in free energy.

Most biological processes are characterised by constant temperature T and pressure p. The appropriate free energy is the Gibbs free energy, which consists of the enthalpy H and the entropy S weighted by the temperature T. The free energy must be minimised for spontaneous directional processes to occur.

$$G = H - TS \qquad (2.2)$$

The bacterial flagellar motor is different from kinesin in that it is powered by the transfer of ions through the cell-membrane, which is an electrochemical rather than a purely chemical process like ATP hydrolysis. Through ion pumps the cell maintains an electrochemical gradient which drives the transfer. The free-energy input from a single ion passing through the cytoplasmic membrane is defined as the elementary charge times the ion motive force (IMF).

$$IMF = V_m + \frac{k_B T}{q} \ln \left(\frac{C_i}{C_o} \right) \qquad (2.3)$$

V_m is the voltage difference across the membrane, with the voltage on the outside subtracted from the voltage on the inside, typically with negative values of V_m under physiological conditions in bacteria. C_i, C_o are the concentrations on the inside and outside respectively, q is the elementary charge, k_B is Boltzmann's constant. Typically the IMF in bacteria is around -150 mV, which yields a free energy of a single ion transit of ~6 $k_B T$.

The two parts of the IMF represent the entropic and the enthalpic term of the free energy, respectively. The entropic component is the chemical potential difference per unit charge due to the concentration difference of ions between the inside and outside of the cell. Ions also carry charges which results in the accumulation of surface charges at the membrane which acts as a capacitor. The voltage arising from these surface charges makes up the enthalpic component of the IMF.

2.5 Modelling

To understand the mechanism of torque-generation in the motor a physical description or model has to be provided. It should explain the coupling of electrochemical transitions to the conformational change that makes the motor move. The most useful framework for descriptions of molecular motors is *Brownian Dynamics*. It involves solving *Langevin* or *reaction-diffusion* equations and is less complex than *Molecular Dynamics* (MD). Thermal fluctuations are modelled by an uncorrelated random force rather than describing every atom in the system like in MD calculations. The degrees of freedom are reduced to those describing mechanical and chemical transitions in the motor. In this framework the motor's work amounts to random-walks down a free energy landscape, see Figure 11.
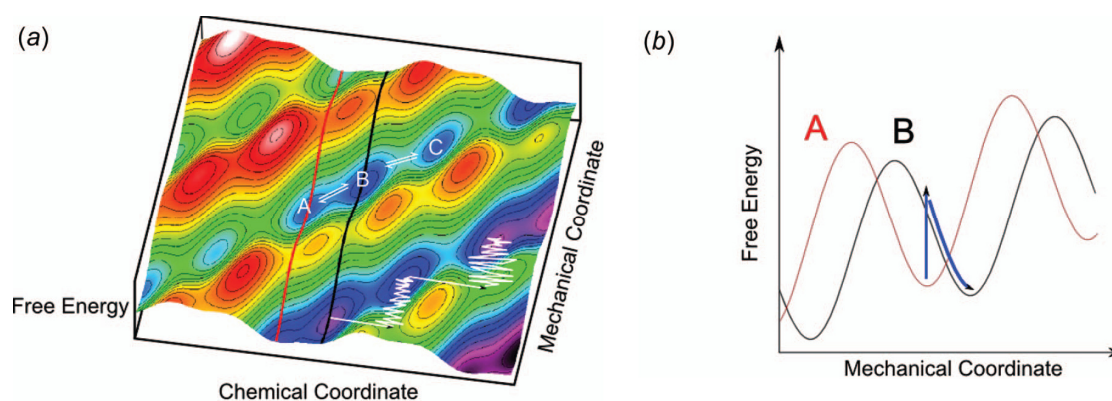

Figure 11: **a,** Free energy landscape with a chemical and a mechanical coordinate. A molecular motor fluctuates between mechanochemical states, which are local minima in the landscape, three of which are labelled A, B and C. The white path in the lower right shows chemical cycles of a motor which are usually characterised by short timescales, followed by diffusion on a longer timescale along the mechanical coordinate towards local minima. **b,** Cross-section of the energy landscape at fixed chemical coordinates. The two energy profiles represent the red and black line through states A and B in (a). In this representation fast chemical transitions amount to a switch from one profile to the other. (Source: [1])

The latest model which was able to explain the torque-speed relationship in the bacterial flagellar motor has been provided by Xing *et al.* [14], see Figure 12.
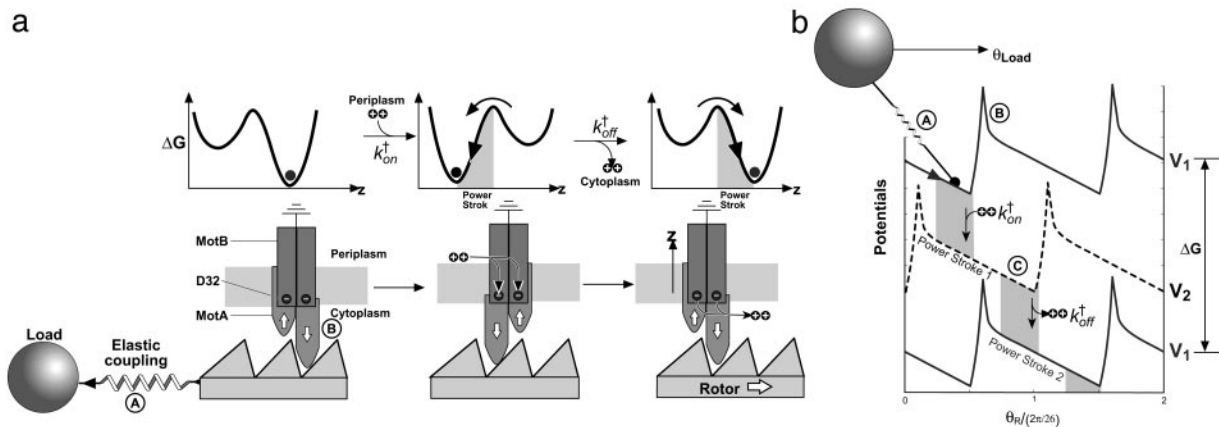
Figure 12: The model for the mechanism of the bacterial flagellar motor as introduced by Xing *et al.* Stator loops interact sterically with the 26 copies of FliG in the C-ring of the rotor. The asymmetry in the steric interaction determines the direction of rotation. **a,** One motor cycle is shown. In the stable configuration at the start of the cycle (lower left) the D32 residues on the stator are unprotonated and the cytoplasmic loop of the MotA unit on the right is extending down, engaging the rotor. Binding of two protons to the MotB D32 residues neutralises them which induces a thermally activated conformational change of the MotA loops, with the left one engaging the rotor and performing a power stroke (lower middle). This process is represented by a transition to a new mechanochemical state, shown for each step in the upper image series which corresponds to energy profiles with respect to motion of the MotA loops along the z-axis. At the end of the first power stroke the bound protons are released into the cytoplasm, triggering a second conformational change. The right MotA loop engages the rotor and performs a second power stroke (lower right). The rate constants k_{on} and k_{off} are composed of the transition rate of the thermally activated conformational change rate and the ion-binding and unbinding rates, respectively. This mechanism is only one out of the possible schemes consistent with the underlying mathematical model. **b,** Sections of the free energy landscape with respect to the angle of rotation. Analogous to Figure 11b the free energy profile is shown for the distinct states in (a) separated by the chemical transitions of ion-binding or unbinding events. The soft elastic coupling between the rotor and load is indicated by a spring A. The peaks labelled as B ensure tight coupling between rotation and proton flux. (Source: [14])

Further data including structural data of the motor units and recordings of rotation and torque of the motor is needed to produce more constrained, realistic models which are consistent with the experimental data, reveal the process-kinetics and allow us to understand the nature of the mechanochemical cycle.

2.6 Measuring rotation of the bacterial flagellar motor

2.6.1 Tethered cell assay

To understand the mechanism of the bacterial flagellar motor its rotation has to be observed experimentally and its torque needs to be measured. Observation and measurement of flagellar rotation however is not easy, because flagellar are too small to be observed by conventional light microscopy.

The first experimental method that allowed observation of the motor rotation was tethering cells to microscope slides with their flagella. The motor has enough power to rotate the entire bacterium, which can be easily observed by light microscopy.

Figure 13: Tethered cell assay

This is how Silverman & Simon were able to prove Berg's theory of bacterial propulsion through flagellar rotation in 1974 [15].
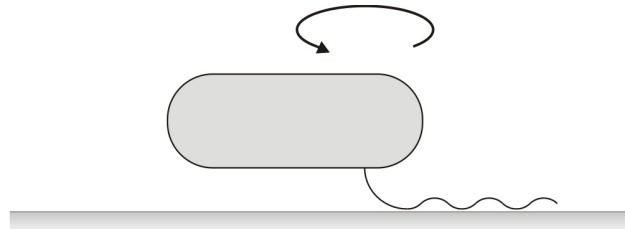
2.6.2 Bead assay

2.6.2.1 Concept

Rotating the entire cell body in the tethered cell assay represents a high-load situation for the motor, far away from natural conditions when rotating flagella. To be able to observe motor rotation at smaller loads the bead assay has been developed. Here cells are immobilised on a microscope slide after

Figure 14: Bead assay

the cells' flagella have been truncated. Subsequently nano-sized beads of various materials, ranging in size from as large as 1 μm down to 60 nm, are attached to the flagellar stub.

2.6.2.2 Optical Trap
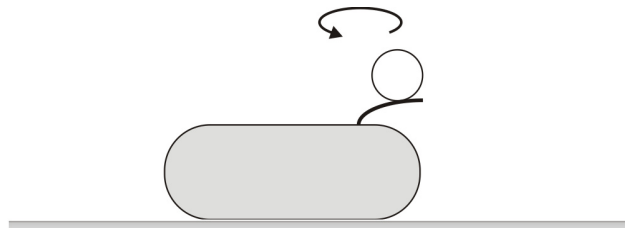
In the standard bead assay polystyrene beads with diameters in the range of 0.25 μm to 1 μm are attached to the flagellar stub. The link between bead and filament is established through a mutated flagellin protein FliC[st] which yields "sticky" filaments that spontaneously bind to surfaces like glass coverslips or polystyrene beads probably through hydrophobic interactions. FliC[st] is a mutated FliC with a deletion in the central region, which probably exposes the hydrophobic core, leading to the interaction described above.

The rotation of the polystyrene bead can be monitored by using an optical trap which, as the name suggests, is used to trap particles. A particle like a polystyrene bead with higher refractive index than its surroundings is exposed to a laser beam with a Gaussian intensity profile. Solving the Maxwell equations gives a net force towards the centre of the beam, see Figure 15.
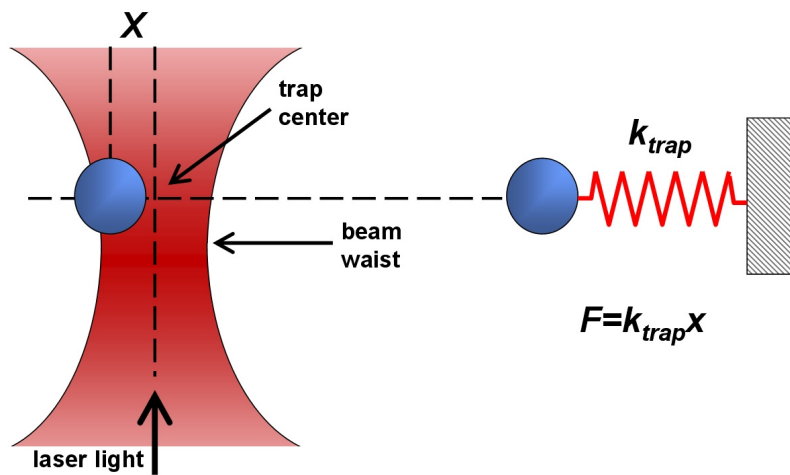
Figure 15: Optical Trap. Dielectric objects are attracted to the centre of the beam. (Source: en.wikipedia.org)

In the bead assay we do not want to trap the particle, but to measure its position. For this a lower laser intensity is used than in trapping mode. Changes in the position of the bead result in changing directions of the laser-light, which can be measured with a quadrant photodiode (QPD).

2.6.2.3 Darkfield

Nan *et al.* introduced a method to look at stepping in the molecular motors kinesin and dynein with high spatial precision and time resolution [16]. An objective-type dark-field microscope is used to track gold nanoparticles attached to these motors. This method can be used to extend observations of rotation in the bacterial flagellar motor to lower load regimes, since it allows observation of particle sizes down to ~60 nm. This is possible due to the strong scattering signal from gold-particles imaged with dark-field microscopy.

60-100 nm gold-beads are attached directly to the bacterial flagellar hook in a strain lacking the filament (*fliC*-deletion). The current method for attachment uses antibody interaction with the primary anti-FlgE antibodies on the hook linked to secondary antibodies on the gold-bead. However this method has been problematic in the past due to low yields of attachment which made collection of sufficiently large amounts of data difficult.

2.7 Stepping rotation

In experiments on ATP-driven motors individual steps of the motors have been observed, giving important information on the mechanisms involved. Observation of

stepping rotation in the bacterial flagellar motor would be similarly beneficial. Through analysis of stepping periodicity information about the site of torque generation can be gathered. Furthermore statistical analysis of stepping data could help in developing more accurate models of the torque-generating mechanism. Unfortunately the observation of steps in the bacterial flagellar motor proved to be difficult due to two factors. In early experiments estimates of the experimental resolution gave a lower bound of 10 steps per revolution [17], thus step sizes are quite small and difficult to observe experimentally. Second, the hook is an elastic structure which smoothes out steps in the rotation of a bead attached to a filament.

In 2005 Sowa *et al.* used relatively small beads (0.2 μm/0.5 μm), attached to Na^+-driven chimeric[1] motors in *E.coli* to observe stepping rotation for the first time, counting 26 steps per revolution [18]. Small beads or low loads mean reduced drag and thus reduced relaxation time of the hook, which should make steps observable. However the speed of the rotation increases, reducing the time in between steps. To overcome this obstacle, lowered rotation-speeds of ~10 Hz were achieved by reducing the number of stators in the motor and reducing the IMF. The number of stators was lowered by expressing stator units at low levels from a plasmid in a strain lacking the stator-genes on the genome. The IMF was reduced by lowering the sodium concentration of the surrounding medium. Reducing the IMF with wildtype motors requires reducing the pH which would have a profound effect on many processes in the cell, making it impossible to observe effects of the reduced IMF alone. This is why stepping could only be observed in Na^+-driven motors so far.

In summary observation of stepping rotation in the bacterial flagellar motor has been limited to the low load and low IMF regime and to Na^+-driven motors.

- To be able to observe stepping rotation with the IMF closer to natural conditions and with wildtype proton-driven motors in *E.coli* the load has to be reduced further. The darkfield setup described above makes observation with smaller bead sizes down to ~60 nm possible and shortens the link between motor and bead via direct attachment of the bead to the hook. However, as mentioned before, the current method of attachment of the beads to the hook via antibody interaction is problematic due to low yields.

---

[1] The BFM of wildtype *E.coli* is proton-driven, but other bacteria have motors driven by sodium-ions. The ion selectivity depends on the stator units of the motor. The stators of *E.coli* (MotA, MotB) are structurally similar to those of the sodium-driven *Vibrio alginolyticus* (PomA, PomB). Asai *et al.* exploited this similiarity and combined parts of MotB and PomB creating PotB, which works in *E.coli* in combination with PomA, allowing observation of rotation driven by sodium-ions. [49]

- For observation of stepping with higher loads the stiffness of the hook needs to be increased.

2.8 Measuring torsional compliance of the flagellar hook

Block *et al.* were able to measure the torsional compliance of the flagellum for the first time in 1989 [19]. Bacterial cells were first tethered to a surface with their flagella as described in Section 2.6.1. The flagellar motors were then locked chemically by treatment with protonophores such as 2,4-dinitrophenol (DNP) or trifluoromethoxycarbonyl-cyanide phenylhydrazone (FCCP), which stops the rotation partially or fully. An optical tweezer was used to rotate the cell, winding up the flagellum. On release the rebound of the cell was recorded. The principle is shown in Figure 16.
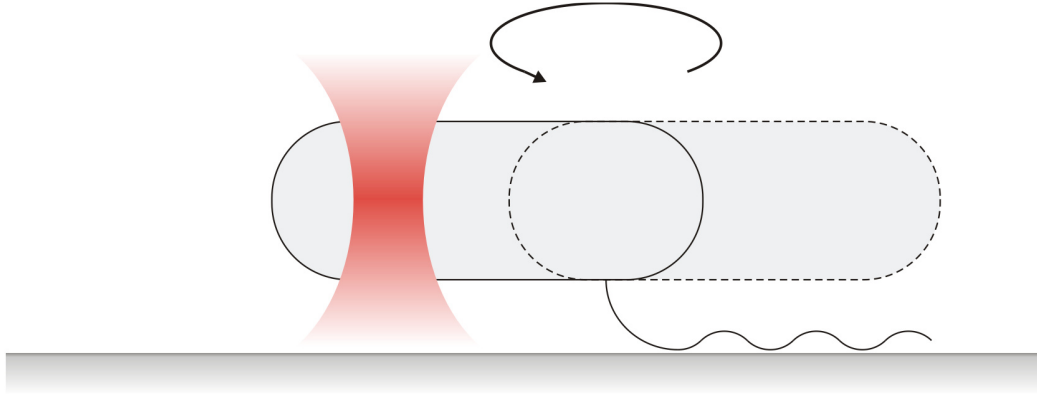
Figure 16: Rotation of a tethered cell with an optical tweezer.

Flagella were attached to the microscope slide by coating the glass surface with anti-FliC antibody which selectively binds FliC, the protein which makes up the filament.

At low Reynolds numbers (usually $\sim 10^{-5}$ for *E.coli*) the torque applied externally is balanced by torques arising from viscous drag on the cell body, torsion in the tether and thermal motion.

$$f_\theta \frac{d\theta(t)}{dt} + k_\theta \theta(t) + L(t) + N(t) = 0 \qquad (2.4)$$

where f_θ is the rotational drag coefficient of the cell body, k_θ is the torsional spring constant of the tether, $\theta(t)$ is its angle, $L(t)$ is the Langevin torque arising from thermal fluctuations of the surrounding medium, $N(t)$ is the applied torque and t is the time.

Assuming that k_θ is constant and neglecting the Langevin torque, this equation can be solved for the rebound event, where $N(t)$ is zero.

$$\theta(t) = Ae^{-\alpha t} \tag{2.5}$$

yielding

$$k_\theta = \alpha f_\theta \tag{2.6}$$

when inserted into equation 2.4. Thus the rebounds can be fitted with an exponential and the time constant of the exponential together with the rotational drag coefficient gives the torsional spring constant.

The geometry of rod-shaped bacterial cells can be approximated by a cylinder. The translational and rotational drag coefficients for cylinders with dimensions of macromolecules were calculated by Tirado & de la Torre [20] [21]. The cells in the tethering assay are however not rotating about the centre of the cell, therefore the equation for the rotational drag coefficient needs to be translated to off-axis geometries [22].

$$f_{r,t} = f_r + f_t d^2 = \frac{\eta \pi L^3}{3(\ln p + \delta_\perp)} + \frac{4\eta \pi L}{\ln p + \gamma_\perp} d^2 \tag{2.7}$$

where f_r is the rotational drag coefficient of the cylinder rotating about its centre, f_t is the translational drag coefficient of the cylinder, d is the distance of the centre of rotation to the centre of the cell. Further quantities on the right include the viscosity of the medium η, the length of the cylinder L, the ratio of length to diameter of the cylinder p and the end-effect corrections $\delta_\perp$ and $\gamma_\perp$ (see [20], [21]).

2.9 Biotin-Streptavidin

Streptavidin is a ~60,000 Da tetrameric protein purified from the bacterium *Streptomyces avidinii*. Its highly specific interaction with biotin (vitamin H) is one of the strongest known non-covalent protein-ligand interactions with the dissociation constant $K_d \cong 10^{-14}$M [23]. It is used widely as a purification and detection system.
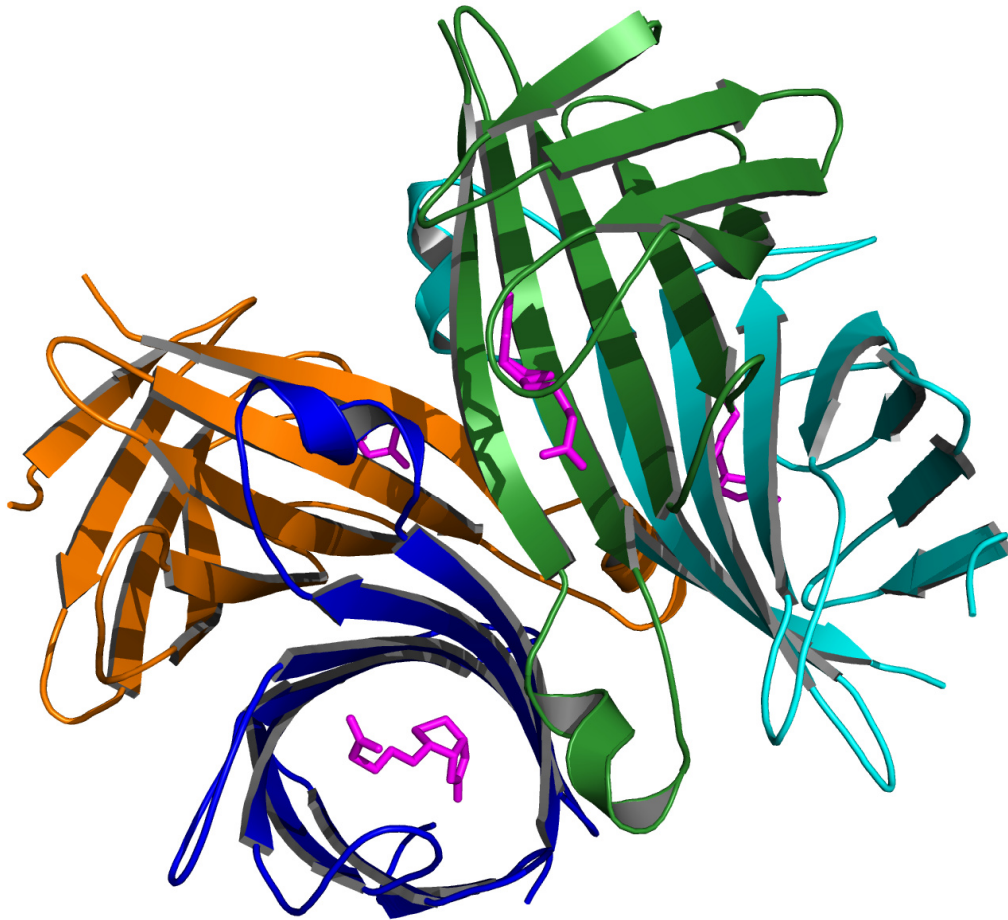
Figure 17: Tetrameric structure of Streptavidin with bound biotin molecules shown in purple and the four subunits shown in orange, blue, green and light blue. (PDB ID: 1SWE)

Covalent linkage of a biotin moiety to a single lysine residue of a specific target substrate is a process called biotinylation and occurs naturally in prokaryotes and eukaryotes. In *E.coli* a subunit of Acetyl-Coa carboxylase (ACC) is subject to post-translational biotinylation. The ACC is a biotin-dependent enzyme, which regulates the metabolism of

fatty acids. Its biotinylation is a substrate specific process which is catalysed by the enzyme BirA.

One way to use biotin to tag a protein, is to insert a peptide into the protein serving as a substrate for biotinylation by BirA. However most proteins would be impeded in their ability to fold and function correctly by the insertion of the large subunit of the ACC. Beckett *et al.* found a short 15-mer peptide, which efficiently mimics the biotin acceptor function of the much larger protein domain normally recognized by BirA [24]. This peptide can be introduced at either the N- or C-terminus of a fusion protein, or at internal protein locations, if the peptide domain is surface exposed and thus accessible to the BirA enzyme.

The advantage of streptavidin labelling over antibody labelling is most evident for proteins at low levels or where long-term imaging is desired [25]. Thus biotinylating the hook protein and using streptavidin-coated gold beads would provide an alternative method of attaching beads to bacterial hooks, possibly giving higher yields of attachment.

Second, the hooks elasticity might be affected by a structural change like the insertion of the biotin accepting peptide (BAP). Binding of streptavidin to a biotinylated hook could also have effects on its elasticity through steric interaction between neighbouring streptavidins. Even cross-linking could occur, due to the fact that streptavidin has four binding sites, see Figure 17. If one streptavidin protein could bind to biotin moieties on two neighbouring FlgE protofilaments they would become cross-linked, which would impair their ability to move against each other.

2.10 Aims of this study

The aims of this study were to

- introduce a biotin tag into the bacterial hook protein which is surface-exposed in the assembled hook structure and retains the hook's function.
- attach streptavidin coated gold-beads to the biotinylated hook for observation of stepping rotation using darkfield-laser-microscopy.
- analyse the effect of streptavidin binding on the compliance of the hook.

3 Materials and methods

3.1 Bacterial strains and plasmids

Information about the strains and plasmids used is provided in Table 1 and Table 2.

E.coli strains	Derived from	Description	Plasmids	Source/Reference
XL1 blue		Strain used for plasmid-DNA amplification with vector pQE60		Stratagene
BW25142		Strain used for plasmid-DNA amplification with vector pDS132. *Pir+* mutant.		[26]
YS34	RP4979 [27]	*⊿cheY, fliC::Tn10, ⊿pilA, ⊿motA, ⊿motB*		[18]
RP437	K-12	Wild-type motile strain.		[28]
MT02	RP437	*fliCst*		Murray Tipping, Department of Biochemistry, University of Oxford. Unpublished
JW1063	K-12	Keio Collection Δ*flgE*		[29]
JW1183	K-12	Keio Collection Δ*ycgR*		[29]
JW1877	K-12	Keio Collection Δ*cheA*		[29]
MTB7	RP437	*flgE*-BAP-siteA		This work
MTB8	RP437	*flgE*-BAP-siteB		This work
MTB9	RP437	*flgE*-BAP-siteC		This work
MTB10	RP437	*flgE*-BAP-siteD		This work
MTB11	RP437	*flgE*-BAP-siteE		This work

MTB18	YS34	Δ*cheY*, Δ*motA*, Δ*motB*, Δ*fliC*, *flgE*-BAP-siteA	pDFB27 (*motA*, *motB*, Arabinose, Amp)	This work
MTB20	YS34	Δ*cheY*, Δ*motA*, Δ*motB*, Δ*fliC*, *flgE*-BAP-siteA	pYS13 (*pomA*, *potB*, IPTG, Chl)	This work
MTB22	YS34	Δ*cheY*, Δ*motA*, Δ*motB*, Δ*fliC*, *flgE*-BAP-siteC	pDFB27 (*motA*, *motB*, Arabinose, Amp)	This work
MTB24	YS34	Δ*cheY*, Δ*motA*, Δ*motB*, Δ*fliC*, *flgE*-BAP-siteC	pYS13 (*pomA*, *potB*, IPTG, Chl)	This work
MTB31	MTB7	Δ*fliC*, *flgE*-BAP-siteA		This work
MTB32	MTB9	Δ*fliC*, *flgE*-BAP-siteC		This work
MTB33	MTB31	Δ*fliC*, *flgE*-BAP-siteA	pYS11 (*fliC*st, Amp)	This work
MTB34	MTB32	Δ*fliC*, *flgE*-BAP-siteC	pYS11 (*fliC*st, Amp)	This work

Table 1: *E.coli* strains used.

Plasmids	Description	Antibiotic resistance	Induced by	Source/Reference
pQE60	Low copy cloning / expression vector.	Amp	IPTG	Quiagen
pDS132	Suicide vector. Cm^R. *sacB*.	Chl	-	[30]
pYS11	*fliC*st	Amp	-	[18]
pYS13	*pomA*, *potB*	Chl	IPTG	[18]
pDFB27	*motA*, *motB*	Amp	Arabinose	[31]

Table 2: Plasmids used.

3.1.1 Storage

The strains were stored in cryotubes at -80ºC. In preparation for storage the strains were grown to stationary phase in Luria-Bertani broth (LB) and mixed with sterile 50% glycerol in a 3:2 ratio.

3.1.2 Growth conditions for cloning

Unless stated otherwise, cells were grown to stationary phase with shaking incubation in LB at 37°C. To select for strains with successfully transformed plasmids, the antibody matching the plasmid encoded resistance was added to the growth medium. Concentrations used are listed in Table 3.

Antibiotic	Concentration
Ampicillin (Amp)	100 μg/ml
Chloramphenicol (Cm)	34 μg/ml

Table 3: Antibiotics used.

The optical density of the bacterial culture was determined by absorption in a Shimadzu UV mini 1240 spectrophotometer at a wavelength of 600 nm.

3.2 Molecular biology

3.2.1 Protein purification

The enzyme biotin ligase (BirA) was expressed and purified following the protocol from Howarth & Ting [25].

3.2.2 DNA preparations

Bacterial plasmid extraction and purification was made using a GenElute plasmid miniprep kit (Qiagen). Chromosomal DNA was extracted and purified using a bacterial genomic miniprep kit (Sigma-Aldrich).

3.2.3 Transforming *E.coli*

The two following methods were used to transform plasmid-DNA in *E.coli* strains.

Strains were made chemically competent using TFB buffers [32]. Transformation in chemically competent cells was performed by heat shock (42°C, 2 minutes) following the protocol by Sambrook *et al.* [32].

Cells were made electrocompetent using GYT-medium [32]. Transformation in electrocompetent cells was performed by electroporation in a Cellject Flowgene electroporator with 2.5kV ~6ms pulses for 2mm gap electrocuvettes or 1,25kV ~6ms pulses for 1 mm gap electrocuvettes. (Protocol by Sambrook *et al.* [32])

Transformed cells were grown on solid LB-agar (1.5% agar) with the appropriate antibiotic at 37ºC overnight. Single colonies were selected and grown in LB at 37ºC while shaking.

3.2.4 Restriction digest

DNA digests were carried out using restriction enzymes from New England Biolabs, provided reaction buffers and, if required, Bovine serum albumin (BSA). Volumes were chosen according to the instructions provided by the manufacturer with final volumes between 20 and 50 μl.

3.2.5 Gel electrophoresis

DNA fragments were separated by gel electrophoresis in 0.5 x TBE buffer with 0.8 – 2.5% (w/v) agarose (Roche), depending on the expected size of the DNA. Electrophoresis was carried out at voltages of 110-150 V. The DNA was mixed with DNA loading dye to help determine the distance covered on the gel. Sizes of the DNA fragments were determined by using a 1 kb or 1 kb plus DNA ladder (Invitrogen). The DNA was visualised by exposure of the gel to ethidium bromide solution for ~20 min, followed by analysis in a Syngene G:BOX gel documentation and analysis system using UV transillumination.

3.2.6 DNA ligation

Ligation of vector and insert DNA (ratio 1:3) was carried out overnight at 16ºC in a reaction volume of 50 μl containing T4 DNA ligase and T4 DNA ligase buffer (New England Biolabs). The ligation mix was then chemically transformed into competent cells (see Section 3.2.3).

3.2.7 PCR

To carry out polymerase chain reactions (PCR) ~100 ng of template DNA, 100 pmol of each primer (Sigma-Aldrich), 12.5 nmol of dNTP mix (Invitrogen) and 1 unit of Pfu DNA polymerase with buffer (Promega) was used in a Techne Techgene thermocycler. Table 4 shows the program used, which is based on the program suggested for use with the Pfu DNA polymerase by Promega. The Annealing temperatue was chosen to be 3-5 degrees below the lowest melting temperature of the primers. An annealing time of 30 seconds was found to be sufficient for plasmid DNA, but genomic DNA required a longer annealing time of 1:30 minutes. The primers used are listed in Appendix B:.

Phase		Temperature [ºC]	Time
Lid preheating		105	Until $T = 105$ºC is reached
Initial denaturation		95	2 min
30 cycles	Denaturation	95	2 min
	Annealing	42-65 depending on T_m of primers	30 sec for plasmid DNA 1:30 min for genomic DNA
	Extension	73	1 min per 500bp of product
Final extension		73	5 min
Final hold		4	∞

Table 4: PCR program

3.2.8 Sequencing

Engineered plasmids were sequenced by the automated DNA sequencing service Geneservice, using BigDye^{TM} dye terminators (PE Biosystems) on a 3730 DNA sequencer (Applied Biosystems). The sequencing data was analysed using the Staden software package and Clone Manager (Sci-Ed Software).

3.2.9 Allelic exchange using pDS132

3.2.9.1 Principle

Several methods are available to introduce mutations in the bacterial chromosomes. One of them is allelic exchange using a so called suicide vector. The goal is to replace a wildtype gene with a mutated version carrying a specific sequence. The desired sequence is introduced into the vector, flanked by up- and downstream regions which are homologous to the wildtype gene, enabling homologous recombination with the genomic DNA. In this study the vector pDS132 is used [30].

The chromosomal replacement is carried out in a two-step process, each involving one homologous recombination, see Figure 18.

To select for the successful recombination in the first step, pDS132 carries chloramphenicol resistance. The vector can't replicate in host cells not expressing a specific protein, hence the term "suicide vector". pDS132 can only replicate in host strains expressing the π-protein, product of the *pir* gene [30]. As the target-strain does not express the π-protein the plasmid cannot replicate and will disappear over time as the cells replicate. Thus using chloramphenicol only selects for the strains where the plasmid has been integrated into the chromosome by homologous recombination.

36

To be able to select for cells which have undergone the second crossover, pDS132 carries a counter-selectable marker. The sacB gene encodes levansucrase, an enzyme which catalyses transfructorylation from sucrose to various acceptors which are lethal for *E.coli* [33]. Growth of the cells in media supplemented with sucrose selects for cells which have undergone the two crossovers and therefore are either correct mutants or wildtype revertants. Screening for the correct mutation is carried out by southern blot or PCR of the genomic DNA.

The advantage of allelic exchange using a suicide vector is that it does not leave an antibiotic resistance marker or a scar on the chromosome like other methods.

Figure 18: Chromosomal replacement by double homologous recombination using the suicide plasmid pDS132. **a,** The first crossover event produces a chromosomal duplication of the homologous gene, one with the desired mutation and one wildtype. **b,** In the second step the duplication is removed by a second crossover between the flanking direct repeats, leaving either the wildtype or the mutated version.

3.2.9.2 Procedure

Recombinant pDS132 carrying a target sequence was introduced into the chosen background strain by electroporation. Electroporated cells were grown on LB agar containing chloramphenicol (Cm) at 37 ℃ for 24-48 hours, which selected for vector integration onto the chromosome. The resulting colonies were grown to stationary phase in LB containing Cm at 37 ℃. 10 μl of the the culture was sub-cultured into 5 ml Sucrose medium (Appendix A) and grown to stationary phase. This step was repeated three times which ensured saturation of sucrose in the cells to select for the second crossover. 1 ml of the final stationary culture was serially diluted 7 times in 10 mM $MgCl_2$ followed by spreading 100 μl of the 10^5, 10^6 and 10^7 dilutions on sucrose medium agar plates. 50 colonies were then picked and each colony is first streaked on a confined, marked position on LB agar plates containing Cm followed by streaking the same colony on a marked position on sucrose medium plates. Only colonies growing on the sucrose medium agar but not on LB agar containing Cm were then grown in LB to saturation. This so called replica plating is an additional control step to ensure that the strains have undergone both crossover events. The genomic DNA of the cultures was extracted with a GenElute™ Bacterial Genomic DNA Kit (Sigma-Aldrich). Gene replacement was confirmed by PCR and sequencing of chromosomal DNA preparations

3.3 Phenotypic analysis & microscopy

3.3.1 Growth conditions

For phenotypic analysis cells were grown at 30℃, shaking at 180 rpm in tryptone-broth (TB) to $OD_{600} = 0.6$.

3.3.2 Swarm plates

The swarm plate assay is a simple method to evaluate a strain's motility and chemotaxis. Petri dishes containing soft agar are prepared using LB with only 0.25% agar. The agar is inoculated with a 5ul drop of bacteria and incubated at 30° for several hours. The bacteria use up nutrient at the site of inoculation, which creates a gradient of nutrient concentration. Thus the chemotactic mechanisms cause them to swarm outwards creating a thin circular disc of bacteria on the agar, the diameter of which gives a measure for motility and chemotaxis of the bacterial strain used.

3.3.3 Epifluorescence

3.3.3.1 Experimental setup

Fluorescence was analysed on a Nikon Eclipse TE2000-E microscope with illumination by a 100 W halogen lamp. Excitation was filtered at 520 nm (bandwidth 30 nm) and emission at 575 nm (bandwidth 50 nm).

3.3.3.2 Visualisation of biotinylated hooks

3.3.3.2.1 Sample preparation
Alexa Fluor® 532 streptavidin conjugate dye (excitation/emission maxima at 532/554 nm) was used to visualise biotinylated hooks using the following protocol. The external biotinylation is based on the protocol by Howarth & Ting [25].

Bacterial cells were grown to OD_{600} = 0.6 in TB. If external biotinylation was required, cells were spun down at 3,400 × g for 2 minutes in a micro-centrifuge and resuspended in ("washed in") 1 ml Motility Buffer supplemented with 5 mM $MgCl_2$ (MB-$MgCl_2$). Two of these washing steps were carried out. In the last step the cells were resuspended in 100 μl MB-$MgCl_2$. ATP (final concentration (f/c) 1 mM), biotin (f/c 10 μM) and BirA (f/c 2 μM) were added, followed by incubation for 20 minutes at room temperature while shaking (100 rpm). Cells were washed twice in MB and resuspended in 150 μl MB. If no external biotinylation was required, cells grown in TB were washed twice in MB and resuspended in 150 μl MB. 100 μl of 1 μM Alexa Fluor® 532 streptavidin conjugate dye was added giving a final dye concentration of 0.4 μM. Incubation was carried out for 20 minutes at room temperature while shaking at 100 rpm. The mix was washed four times in MB to remove residual dye from the sample. To immobilise the cells 1 μl of the sample was then pipetted on an agarose slide.

3.3.3.2.2 Agarose slide preparation
Milli-Q water was supplemented with 1.2% of agarose. ~100 μl of melted agarose solution was pipetted onto a microscope slide in between 2 coverslips about 1 cm apart. A third coverslip was pressed down on the coverslips and the drop to create a thin film of agarose-gel. When cooled down a 1 μl drop of bacterial sample in solution was pipetted onto the agarose-gel layer and covered with a coverslip.

3.3.3.3 Visualisation of free swimming bacteria

3.3.3.3.1 Sample preparation

The preparation of samples for visualisation of cells and flagella is based on the protocols used by Darnton *et al.* [34] and Turner *et al.* [35]. The external biotinylation is based on the protocol by Howarth & Ting [25].

Bacterial cells were grown to $OD_{600} = 0.6$ in TB. Cells were spun down at $3,400 \times g$ for 2 minutes in a micro-centrifuge and resuspended in ("washed in") 1 ml Motility Buffer supplemented with 5 mM $MgCl_2$. Two of these washing steps were carried out. In the last step the cells were resuspended in 100μl MB-$MgCl_2$. ATP (f/c 1 mM), biotin (f/c 10 μM) and BirA (f/c 2 μM) were added, followed by incubation for 20 minutes at room temperature while shaking (100 rpm). Cells were washed twice in MB and resuspended in 100 μl MB. If required, streptavidin was added with a final concentration of 20 μM, followed by incubation for 15 minutes while shaking (100 rpm). Cells were washed twice and resuspended in 100 μl MB (pH 7.5). 5 μl of 1.0 M sodium hydrogen carbonate was added to reach pH ~8 (labelling efficiency is higher at higher pH). 60 μl of MB (pH7.5) was added to one package of Cy3 monofunctional succinimidyl ester (PA23001, Amersham/GE Healthcare, excitation/emission maxima at 550/570 nm). 10 μl of dye in suspension was then added to each bacterial sample. The samples were incubated for 90 minutes while shaking at 100 rpm in the dark. Excess dye was removed by washing three times in MB+ (MB supplemented with 0.5% glucose and 0.002% Tween20 (Sigma-Aldrich)). Cells were resuspended in 1-2 ml of MB+.

3.3.3.3.2 Slide preparation

For observation about 40 μl of bacterial solution was sealed within a ring of vacuum silicone grease (VWR International) between a coverslip (22x22 mm) and a microscope slide.

3.3.4 Dark field microscopy

3.3.4.1 Experimental setup

In dark field setups for tracking gold nanoparticles usually the forward scattered light is collected. [16] [36] In the custom built setup used here samples are illuminated from below due to the higher scattering cross section for back-scattered light, with the laserlight passing through the objective first, see Figure 19. The back-scattered light is collected and imaging is performed on a high speed camera (Photron FASTCAM-X 1024 PCI) at a framerate of up to 109.5 kHz.
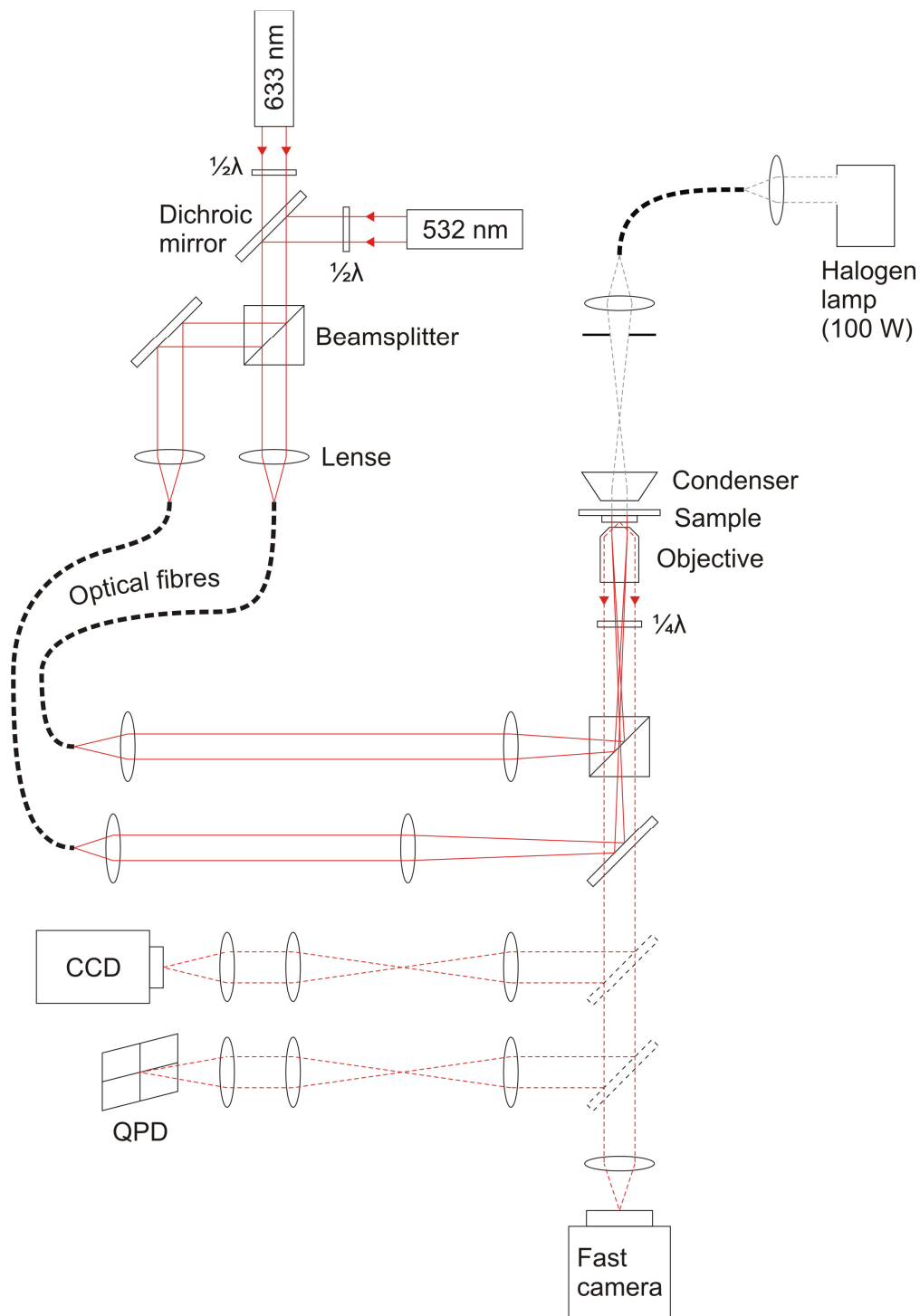
Figure 19: Layout of the dark field setup. A 633 nm HeNe or a 532 nm Nd:YAG laser are used for dark field imaging with a 100x NA 1.3 objective. The backscattered light is collected and either anaylsed with a QPD for preliminary detection of rotation or recorded with a Photron Fastcam-X 1024 PCI. Köhler illumination with a 100W Halogen lamp and a high numerical aperture condenser were used for bright field imaging with a CCD camera.

3.3.4.2 Sample preparation

3.3.4.2.1 Gold streptavidin conjugation
Streptavidin conjugated gold colloids were prepared following the protocol of Furuike, *et al.* [37]. The following buffers were used.

- Buffer A: 10 mM MOPS (3-(N-morpholino)propanesulfonic acid)-KOH, pH 7.0, 50 mM KCl, and 2 mM MgCl2.
- Buffer B: Buffer A without MgCl2.

5 μl of 100 μM Streptavidin in Buffer A, 5 μl of 0.5mM dithiobis[succinimidylpropionate] (DSP) in Buffer B and 5 μl of 10mM tris(2-carboxyethyl)phosphine (TCEP) in buffer B was added to 1 ml of 100-nm gold beads (BBInternational, Corpuscular). After incubation for 2 hours at room temperature in a rotating mixer the sample was incubated for 12-48 hours at 4 °C, again in a rotating mixer. Samples were stored at 4 °C.

3.3.4.2.2 Gold preparation
300 μl of streptavidin conjugated gold beads (diameter 60 or 100 nm) were washed (3,400 × g, 1 min) three times in 300 μl 10 mM Tris (pH 8) or 10 mM HEPES (pH 7.3). The bead pellet was not resuspended after the last spindown.

3.3.4.2.3 Cell preparation
The external biotinylation is based on the protocol by Howarth & Ting [25].

Bacterial cells lacking filaments were grown to OD_{600} = 0.6 in TB. Cells were spun down at 3,400 × g for 2 minutes on a tabletop centrifuge and resuspended in ("washed in") 1 ml Motility Buffer supplemented with 5 mM MgCl2. Two of these washing steps were carried out. In the last step the cells were resuspended in 100 μl MB-MgCl2. ATP (f/c 1 mM), biotin (f/c 10 μM) and BirA (f/c 2 μM) were added, followed by incubation for 20 minutes at room temperature while shaking (100 rpm). Cells were washed twice in MB and resuspended in 100 μl. The bacterial suspension was added to the gold-pellet and mixed by pipetting, followed by 30 minutes incubation at room temperature while shaking at 100 rpm. To remove residual unbound gold, the cell-goldbead mix was spun down at 1,800 × g for 45 seconds and the supernatant was removed carefully by pipetting. The cells were then resuspended in 100 μl MB.

3.3.4.2.4 Slide preparation
Using double-sided adhesive tape, microscope slides and coverslips (22 x 22 mm) a so called tunnel slide can be prepared, see Figure 20. For immobilisation of the bacterial cells a 0.01% Poly-L-lysine solution is flown in and incubated for 1 min. Polylysine, a synthetical polypeptide, is positively charged and can thus be used to coat the negatively

charged glass surface. Attachment of the bacterial cells to the polylysine layer occurs due to the negative charges on the outer membrane of *E.coli*.
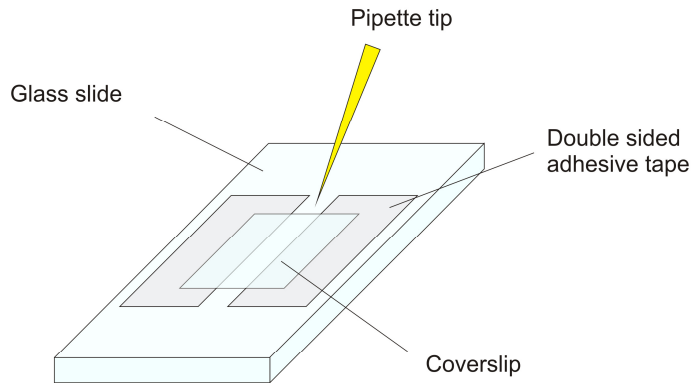
Figure 20: Tunnel slide. The central chamber has a volume of ~ 10 μl.

Washing is performed by flowing through 50 μl MB. The prepared cell-gold mix is flown in with following inverted incubation for ~10 minutes. Amounts of cells stuck to the coverslip can be controlled by adjusting the incubation time after checking the cell-number by light microscopy. Another washing step with MB is carried out after which the tunnel ends are sealed with grease.

3.3.5 Optical trap

3.3.5.1 Experimental setup

The layout of the optical trap is shown in Figure 21. It consists of a custom-built inverted microscope and two lasers, a 632 nm Helium Neon (Coherent, USA) and a 1064 nm Ytterbium fibre laser (IPG Photonics Corporation, USA). Position detection in the bead assay is done by Back Focal Plane (BFP) interferometry using one of the two lasers focused into the specimen plane by the objective and collimated by the condenser onto the face of a quadrant photodiode in the BFP of the condenser.
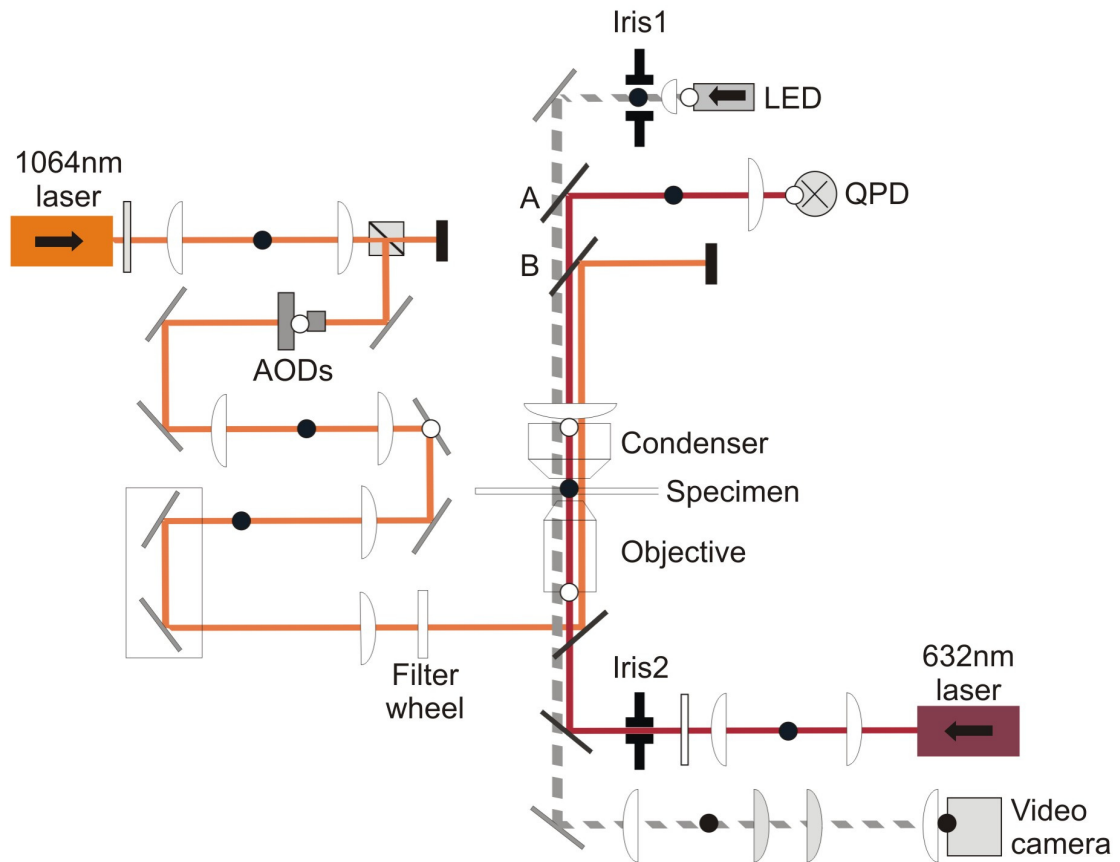
Figure 21: Layout of the optical trap. Bright-field imaging uses an LED, high numerical aperture condenser, 100X oil-immersion objective and a high-sensitivity CCD video camera (LCL-902K, Watec). The 632 nm laser is only used for detection of rotation in the bead assay. The filter wheel allows reduction of laser power with one of two neutral density (ND) filters (ND = 1 and ND = 0.5). The 1064 nm laser can be used for either position detection in the bead assay or for trapping. Data acquisition and fine control of the trapping laser is achieved with an Acousto-Optic Deflector (AOD) controlled by a Digital Signal Processing (DSP) board. The intensity of the 1064 nm laser was varied via the laser diode current. (Source: [38])

3.3.5.2 Bead assay

3.3.5.2.1 Polystyrene bead preparation
Polystyrene beads with a diameter of 0.5 μm (Bangs Laboratories, Inc.) at 1% (w/v) were diluted 1:10 in MB.

3.3.5.2.2 Cell Preparation
The external biotinylation is based on the protocol by Howarth & Ting [25].

Bacterial cells lacking filaments were grown to $OD_{600} = 0.6$ in TB. Cells were spun down at $3,400 \times g$ for 2 minutes on a tabletop centrifuge and resuspended in ("washed in") 1

ml Motility Buffer supplemented with 5 mM $MgCl_2$. Two of these washing steps were carried out. In the last step the cells were resuspended in 100 µl MB-$MgCl_2$. ATP (f/c 1 mM), biotin (f/c 10 µM) and BirA (f/c 2 µM) were added, followed by incubation for 20 minutes at room temperature while shaking (100 rpm). Cells were washed twice in MB and resuspended in 250 µl.

3.3.5.2.3 Slide preparation

The channel of a tunnelslide is filled with Poly-L-lysine followed by inverted incubation (coverslip facing down) for 1 minute. Washing is performed by flowing through 50 µl MB. The bacterial suspension is flown in with following inverted incubation for ~10 minutes. Amounts of cells stuck to the coverslip can be controlled by adjusting the incubation time after checking the cell-number by light microscopy. The channel is washed by flowing through 50 µl MB. 10 µl of the prepared polystyrene beads in solution are flown in followed by 10 minutes of inverted incubation. Washing is again performed by flowing through 50 µl MB, after which the tunnel ends are sealed with grease.

3.3.5.3 Tethering assay

3.3.5.3.1 Cell Preparation

The external biotinylation is based on the protocol by Howarth & Ting [25].

Bacterial cells carrying the *fliCst*-mutation were grown to $OD_{600} = 0.6$ in TB. The sticky filament phenotype allows attachment of the bacterial cells to the glass coverslip with their flagella without using anti-FliC antibody. Cells were spun down at 3,400 × g for 2 minutes on a tabletop centrifuge and resuspended in ("washed in") 1 ml Motility Buffer supplemented with 5 mM $MgCl_2$. Two of these washing steps were carried out. In the last step the cells were resuspended in 100 µl MB-$MgCl_2$. ATP (f/c 1 mM), biotin (f/c 10 µM) and BirA (f/c 2 µM) were added, followed by incubation for 20 minutes at room temperature while shaking (100 rpm). Cells were washed twice in MB and resuspended in 100 µl. Streptavidin was added with a final concentration of 20 µM, followed by incubation for 15 minutes while shaking (100 rpm). Cells were washed twice in MB and resuspended in 250 µl.

3.3.5.3.2 Slide preparation

The bacterial suspension is flown in a tunnel slide with following inverted incubation for ~10 minutes. Amounts of cells stuck to the coverslip by their flagella can be controlled by adjusting the incubation time after checking the cell-number by light microscopy. Washing is performed by flowing through 50 µl MB.

The slide is mounted on the optical trap setup. Once a spinning tethered cell is found buffer containing 0.1 % glutaraldehyde is flown in to lock the motor and stop rotation[2].

---

[2] To lock up the motor Block & Berg used protonophores which lead to fully locked, partially locked and freely rotating cells. In a second publication following the one introducing this experiment Block & Berg used gentle fixation by 0.1% glutaraldehyde which is a more reliable procedure to lock up the motor. They concluded that glutaraldehyde does not significantly change the properties of the hook. This is why fixation by 0.1% glutaraldehyde is used here.

4 Experiments and results

4.1 Biotinylation of the hook-protein

4.1.1 Sites of insertion

The aim of this study was, as outlined in Section 2.10, to introduce a biotin tag into the bacterial hook protein which is surface-exposed in the assembled hook structure and retains the hook's function.

To use the 15-mer biotin acceptor peptide (described in Section 2.9) for purification or tagging purposes, the DNA-sequence encoding for it is usually added to the C- or N-terminus of the protein in question. This way the protein is most likely to support the insertion, folding to its native state without its function being impaired. In this study however we are not dealing with single proteins, but a protein-complex made up of ~120 FlgE proteins, called protofilaments of the structure. To introduce a biotin tag into this structure, the insertion sites have to be carefully chosen so that the tag is surface exposed.

Fujii *et al.* resolved the structure of FlgE in the assembled hook of *S. typhimurium* [7]. This structure is useful for the selection of insertion sites in FlgE of *E.coli* as well, since the proteins in the two related species show 88% homology. Figure 22a, b and c show three dimensional density maps of the hook with the fitted atomic model. FlgE in *E.coli* is composed of 402 amino acids. As can be seen in Figure 22b only domain D2, a central segment from A146 to K284, lies on the outside of the assembled hook structure. Therefore the peptide cannot be attached terminally or the biotin tag would be buried and inaccessible. Successful insertion of the biotin accepting peptide in non-terminal regions has been achieved previously [39] [40] [41] and it seems that insertion is most likely to be supported in loops. Shaik *et al.* compared sequence identity in FlgE for 13 bacterial species [42]. The protein is most likely to support insertion while retaining its function in regions of low identity among species. Based on this data and the three dimensional structure of FlgE when assembled in the hook complex, five insertion sites for the biotin accepting peptide were chosen, three of which are in loops, see Figure 22d and Table 5
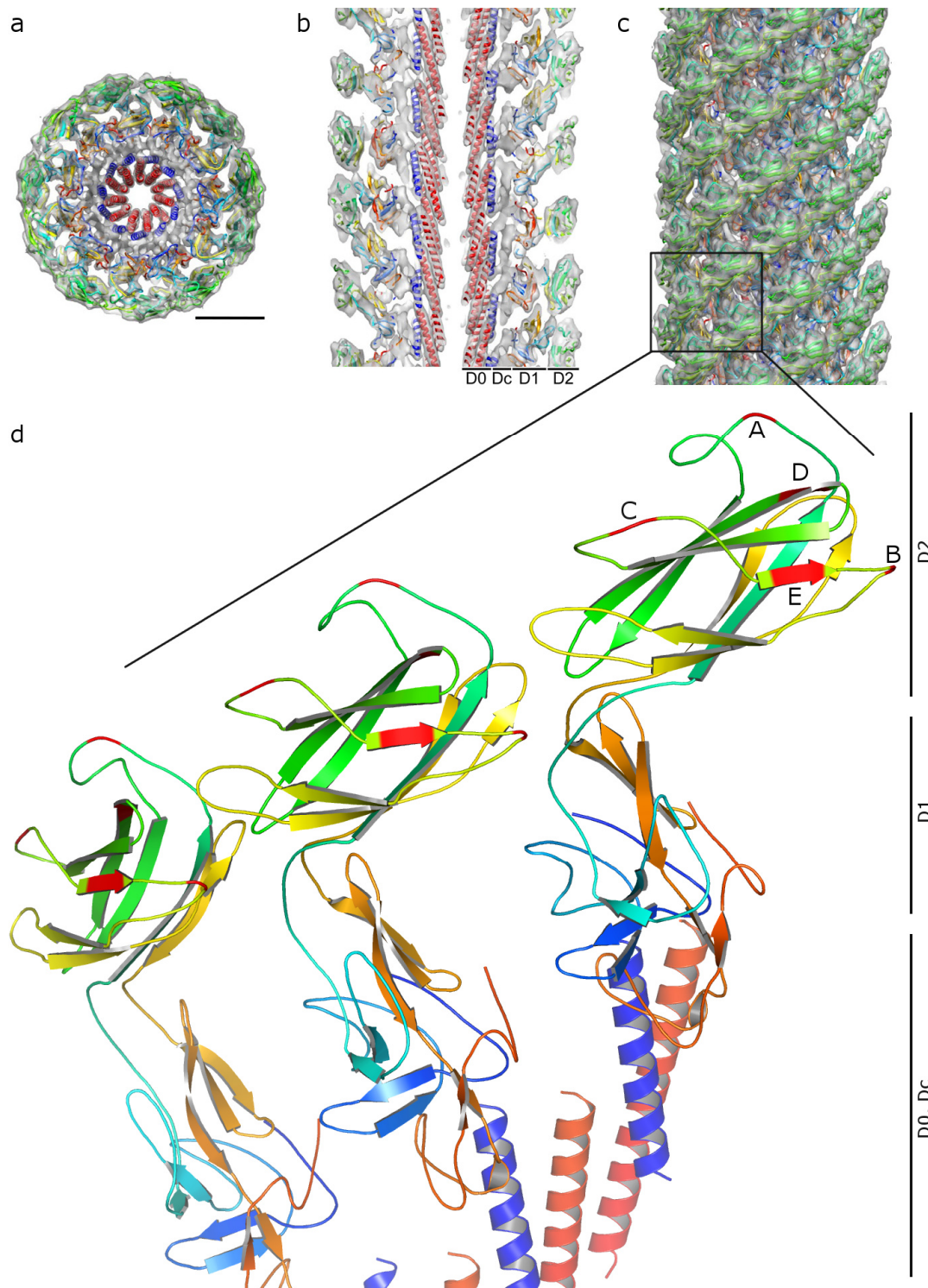
Figure 22: **a, b, c,** Three-dimensional density maps of the hook with a fitted atomic model, showing the hook perpendicular to (a) and along its longitudinal axis (b, c), cross-section (b) and outer structure (c), respectively. Scale bar, 50 Å **d,** Structure of three FlgE protofilaments with the insertion sites for the biotin accepting peptide marked in red and labelled A through D. (Source: [7], PDB ID: 3A69)

Insertion Site	Position (*S.typhimurium*)	Position (*E.coli*)	Working name
A	S166 – K167	T166 – V167	Site 1
B	E234 – N235	A232 – N233	Site 2
C	T221 – A222	I221 – A222	Site 4
D	K202 – T203	K202 – T203	Site 6
E	T229 – L230	T227 – L228	Site 11

Table 5: Biotin acceptor peptide insertion sites in FlgE.

4.1.2 Plasmid expression

Using PCR a vector-construct was made containing the 1206 bp *flgE*-gene which encodes for the protein FlgE. The template was genomic DNA of the *E.coli* wildtype strain RP437. The primers contained restriction sites for the restriction enzymes NcoI and BamHI, which allowed insertion of the construct into the multiple cloning site of the vector pQE60.

The five insertion sites for the biotin acceptor peptide all are in a central segment of *flgE* which is enclosed by two restriction sites for the restriction enzymes ClaI and AleI. Five oligonucleotide-sequences of this 249 bp segment were ordered from Entelechon (www.entelechon.com), each containing an acceptor peptide at one of the insertion sites. They were ligated into the *flgE*-pQE60 vector construct, which was then checked by PCR and sequencing. The generic construct showing all five sites is shown in Figure 23.
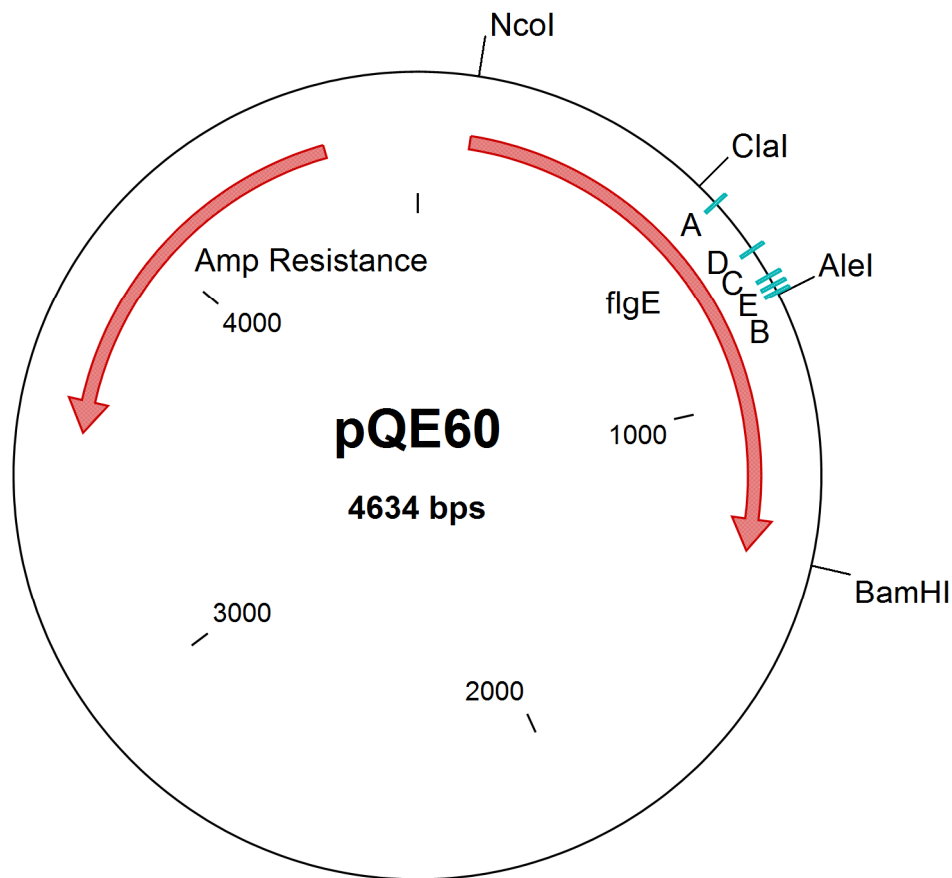
Figure 23: pQE60 vector construct with the five insertion sites shown (A-E).

The vector constructs carrying the BAP (biotin acceptor peptide) at the individual insertion sites were then transformed into a strain carrying a *flgE*-deletion, obtained from the Keio collection [29]. This strain is of course non-motile, since lack of FlgE prevents assembly of the hook and thus the whole flagellum. Expression of FlgE-BAP was then induced by supplementing the growth medium with Isopropyl β-D-1-thiogalactopyranoside (IPTG) at a final concentration of 50 μM.

If the engineered hook-protein is not impaired by the insertion it should be exported as normal, resulting in flagellar formation and restoration of motility.

Motility was checked with a commercial phase contrast light microscope. It was found that the neither the expression of FlgE-BAP nor of wildtype FlgE complemented the deletion. Full induction was made sure by raising the IPTG concentration to 1 mM without any change in motility.

Possible reasons include

- Formation of unnaturally long hooks, so called "polyhooks", which are known to occur at high expression levels of FlgE.
- The *flgE*-deletion in the Keio strain caused polar effects on expression of genes downstream.

Due to the fact that plasmid-expression of wildtype FlgE did not complement the FlgE deletion the only way to incorporate FlgE with the inserted BAP in the bacterial flagellar hook was to replace the *flgE*-gene on the chromosomal DNA.

4.1.3 Genomic replacement

Genomic replacements of the *flgE*-gene with the *flgE-BAP* sequence was carried out in the wildtype strain RP437 using the suicide vector pDS132 (see Section 3.2.9). Screening for the mutation was performed by PCR followed by gel-electrophoresis (Exemplary result shown in Figure 24). Successful mutations were confirmed by sequencing the full *flgE* PCR product.
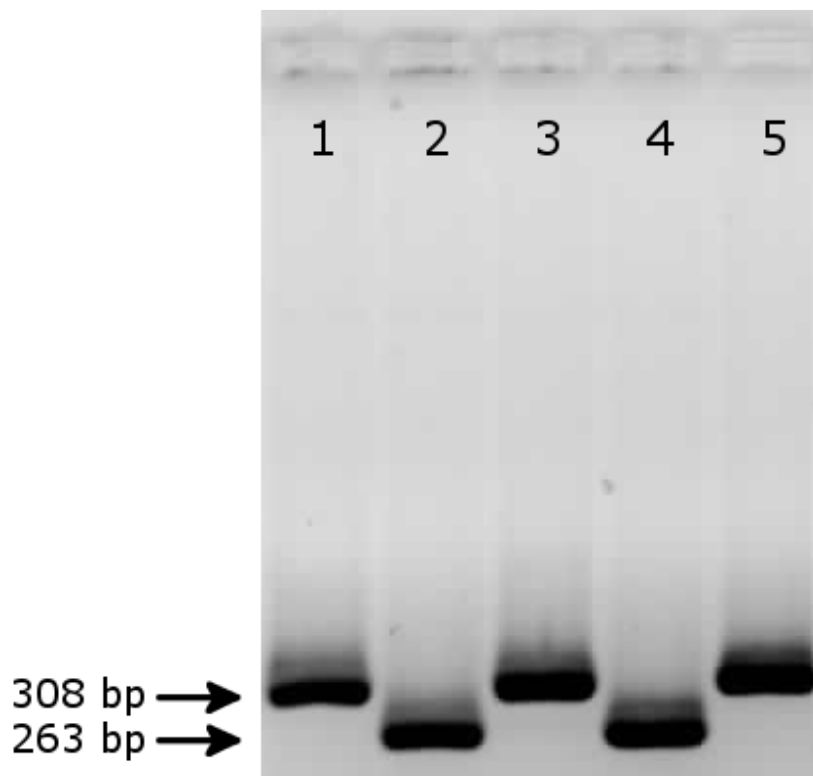
Figure 24: Agarose-gel showing the insertion of the 45 bp BAP sequence, checked by PCR of a 308 bp sequence in successfully mutated strains (1, 3 and 5) or 263 bp in wildtype revertants (2 and 4). Greyscale inverted; Primers: FlgE_BAP_test_Fwd2, FlgE_BAP_test_Rev2.

The strains were characterised by analysis of motility to assess successful assembly of the hook with the engineered hook-protein.

The genomic replacement was then carried out in the strain YS34 which lacks filaments, this time only for the insertion sites A and C due to the results of the motility and fluorescence analysis in the following sections. This strain can be used for experiments with attached gold-beads on the dark field microscopy setup. By transformation with a plasmid expressing sticky FliCst the strain can also be used for experiments with attached polystyrene beads on the optical trap setup. Expression of FliCst also allows measurement of the torsional compliance of the hook in the tethering assay, again using the optical trap.

4.2 Motility analysis

4.2.1 Free swimming

Motility of the strains MTB7, MTB8, MTB9, MTB10 and MTB11, each carrying the *flgE-BAP* mutation for one of the five sites, was checked by light-microscopy. Since these strains are derived from wildtype RP437, they should be motile if the hook can be assembled with the mutated hook-protein.

Only the strains carrying the mutation at insertion sites C (MTB9) and E (MTB11) were found to be motile.

4.2.2 Swarm plate assay

The swarm plate assay was used to quantify the motility of the engineered strains. Normally the swarming assay tests both motility and chemotaxis, however the strains used here have no alterations in genes involved in chemotaxis. Thus the assay can be used to assess motility. Nine swarming plates were analysed for each strain with 3 repeats of 3 independent cultures per strain. Swarming of the different strains on one of the plates is shown in Figure 25. The strains are labelled by their individual insertion sites for the *flgE-BAP* mutation.
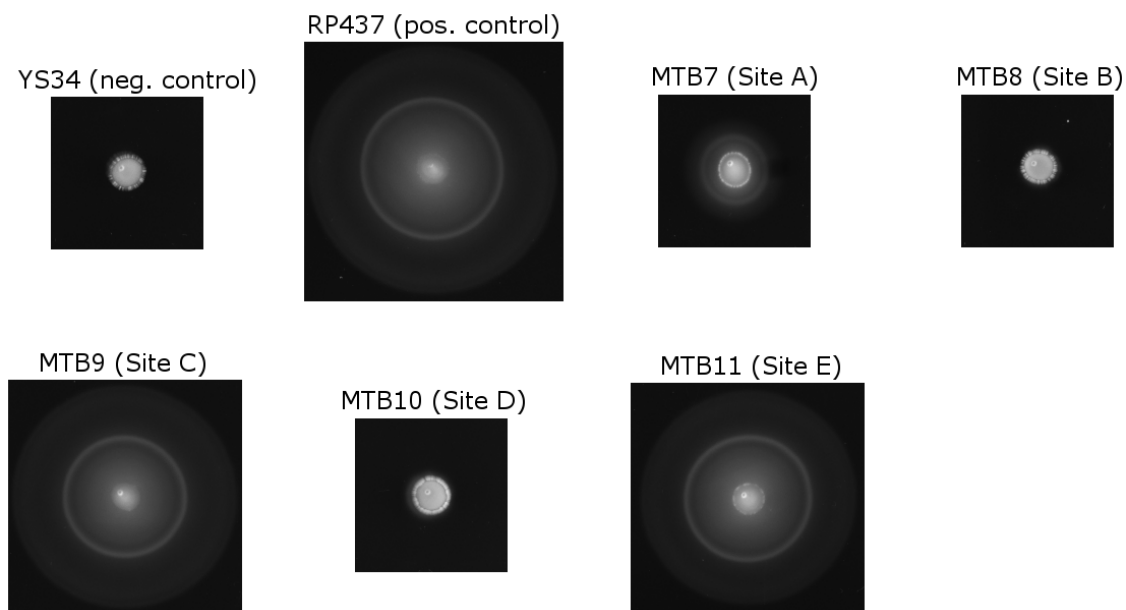
Figure 25: Swarm diameters. A non-motile negative control (YS34), a fully motile positive control (RP437) and the 5 engineered strains are shown.

The diameters of the swarmed cultures were measured and the averages for each strain computed, see Figure 26.
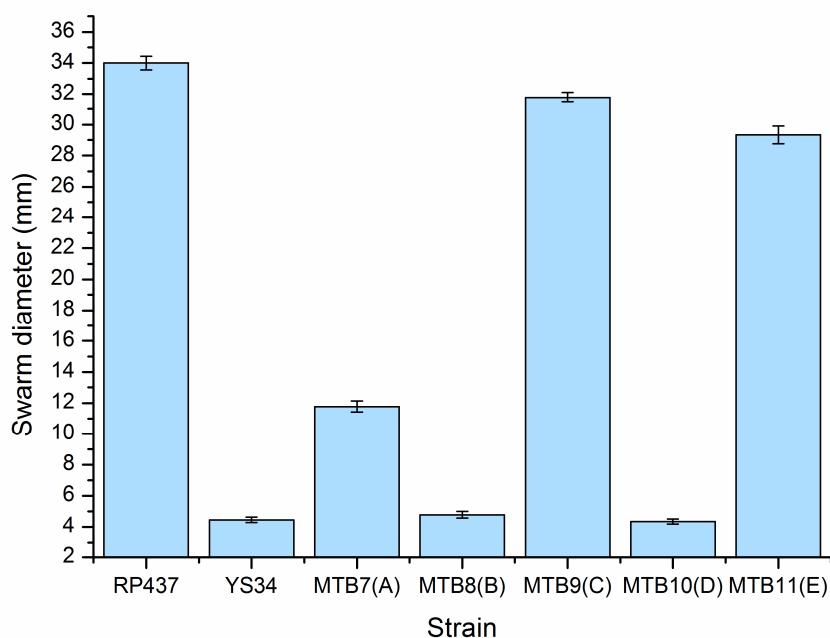
Figure 26: Swarm diameters, averaged from 9 samples. Error bars show the standard error. RP437 is the fully motile positive control. YS34 is the non-flagellated and thus non-motile negative control. Strains with the BAP insertion at site C and D are almost fully motile (92% and 84%), whereas insertion at site A leaves only partial motility (25%) and insertions at site B and E result in the complete loss of motility.

The swarming diameters suggest that some of the insertions are supported, however all of them seem to have an effect on motility. As the insertions at site B and C result in a complete loss of motility, they could possibly even prevent hook formation. To assess the effects of the mutation further analysis of the strains was necessary.

4.3 Confirmation of biotinylation by fluorescent labeling

Invitrogen Alexa Fluor® 532 streptavidin conjugated dye was used to confirm successful biotinylation of the hook on the epifluorescence setup. The five strains carrying the biotin accepting peptide at the individual insertion sites were compared and the result is shown in Figure 27.
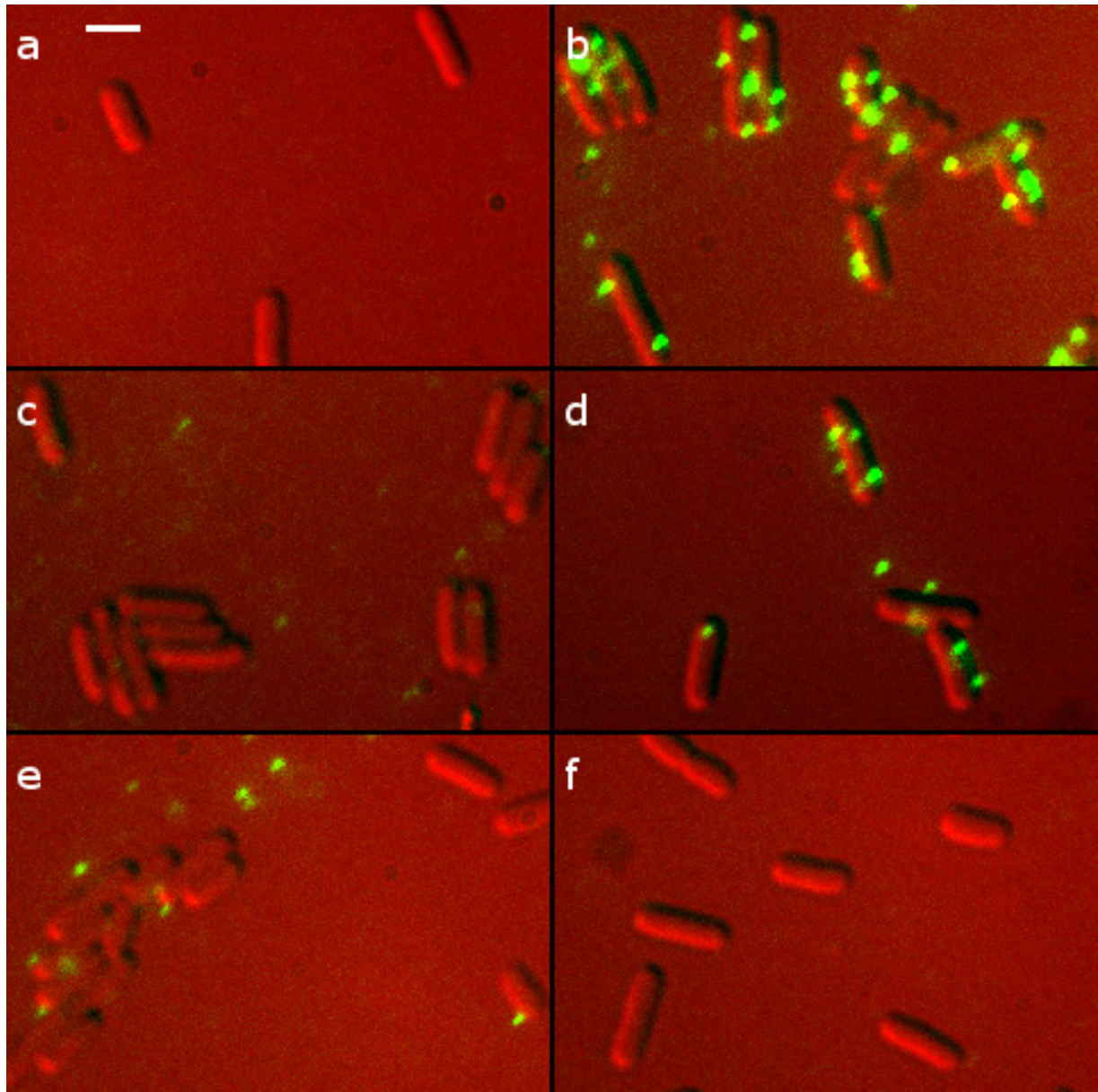
Figure 27: Epifluorescence images of Alexa Fluor® 532 streptavidin conjugated dye attached to the biotinylated hooks. The DIC image (red) is overlayed by the fluorescence channel (green). Fluorescence exposure time 300 ms. The fluorescence channel has been contrast enhanced. External biotinylation was performed on all the strains to maximise attachment of dye and fluorescent signal. **a,** RP437 wildtype (negative control) showing no signal **b,** MTB7 (*flgE*-BAP-siteA). Distinct spots on each cell show the position of the bacterial flagellar hooks. The strong signal indicates successful biotinylation **c,** MTB8 (*flgE*-BAP-siteB) showing no signal on the cells. **d,** MTB9 (*flgE*-BAP-siteC) shows a strong signal, indicating biotinylated hooks **e,** MTB10 (*flgE*-BAP-siteD). Signals not localised on the cells can be observed, possibly due to disintegrating hooks. **f,** MTB11 (*flgE*-BAP-siteE) shows no signal. Scale bar, 1 μm.
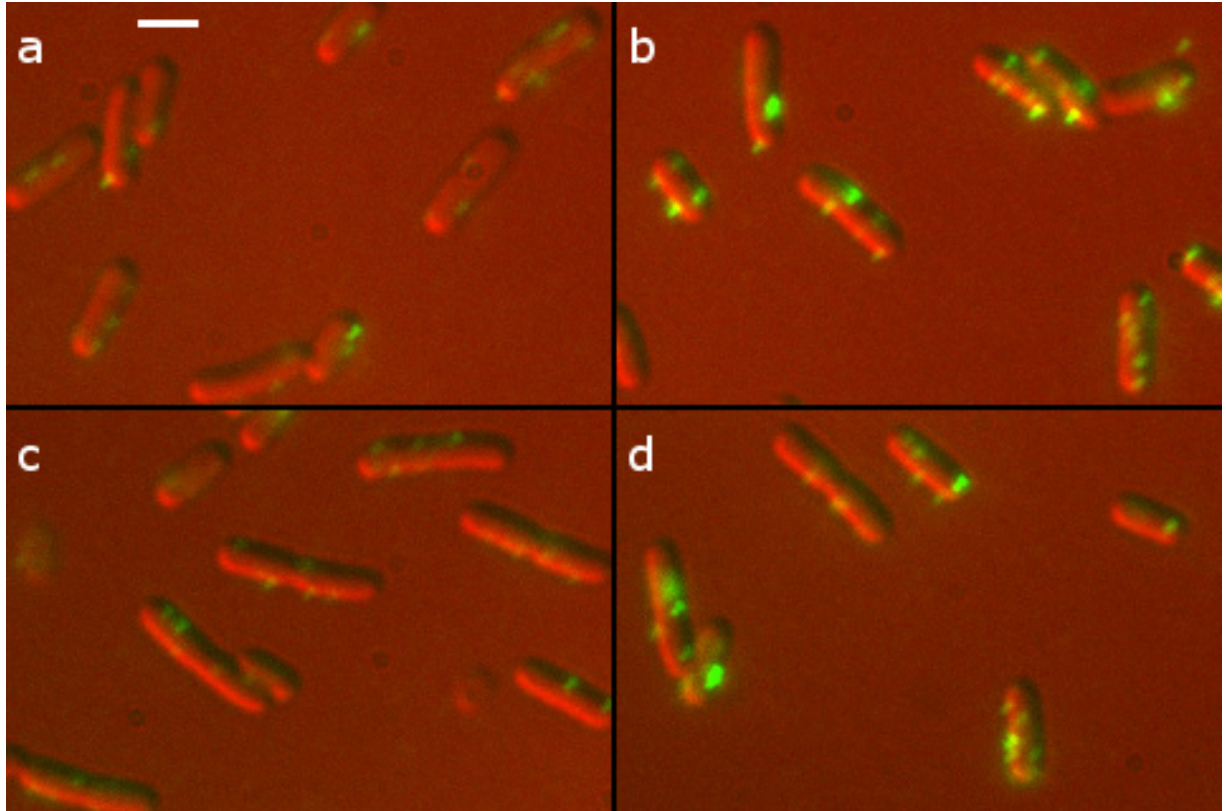
Figure 28: Epifluorescence images of Alexa Fluor® 532 streptavidin conjugated dye attached to the biotinylated hooks. The DIC image (red) is overlayed by the fluorescence channel (green). Fluorescence exposure time 400 ms. Natural occurring biotinylation (left) versus additional external biotinylation (right) is shown. **a, b,** MTB7 (*flgE*-BAP-siteA) **c, d,** MTB9 (*flgE*-BAP-siteC). External biotinylation results in higher dye-attachment yields. Site A and C show equal levels of fluorescence. Scale bar, 1 μm.

Based on the results of the fluorescence assay the insertion sites A and C have been selected for further experiments. Surprisingly the 84% motile strain MTB11 (Site E) didn't show any biotinylation. A possible reason is the integration of the BAP in a beta sheet at insertion site E, which could prevent either the biotin from being accessible for streptavidin or the BAP from being accessible for biotinylation. The strains MTB20 and MTB24 (BAP insertion at site A and C in YS34) were analysed in the fluorescence assay as well, yielding a positive result, which confirmed maintained biotinylation levels in strains lacking filaments (data not shown).

4.4 Bead assay

4.4.1 Light microscopy

Preliminary experiments to assess bead-attachment to biotinylated hooks in the strains MTB20 (Site A) and MTB24 (Site C) with 1 μm streptavidin-conjugated polystyrene beads (Bangs Laboratories, Inc.) were successful. Beads of this size can easily be observed with a conventional phase-contrast light microscope. However yields of attachment were lower than the yields obtained by conventional attachment of beads to filaments using sticky FliC[st].

4.4.2 Optical trap

Rotation of streptavidin-conjugated polystyrene beads with a diameter of 0.5 μm attached to the biotinylated hook of the strain MTB24 (Site C) were recorded in the optical trap setup. Speeds were fairly constant at a speed of ~75 Hz with some sudden stops, see Figure 29.
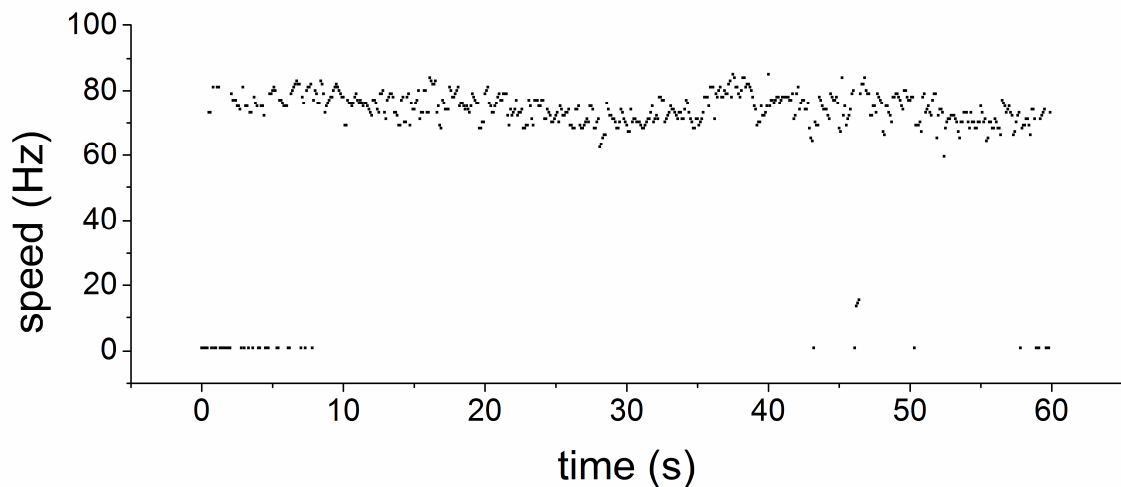
Figure 29: Speed-time plot for the rotation of a 0.5 μm streptavidin-conjugated polystyrene bead, attached to the biotinylated hook of the strain MTB24 (Site C).

4.4.3 Dark field microscopy

Gold-bead rotation experiments were carried out on the dark field setup mainly with the chimeric strains MTB20 (BAP at site A) and MTB24 (BAP at site C). These strains carry a *fliC*-deletion, are non-switching (only CCW rotation due to *cheY*-deletion) and their motors are driven by Na^+-ions. The chimeric stators are expressed from a plasmid with the inducer IPTG.

58
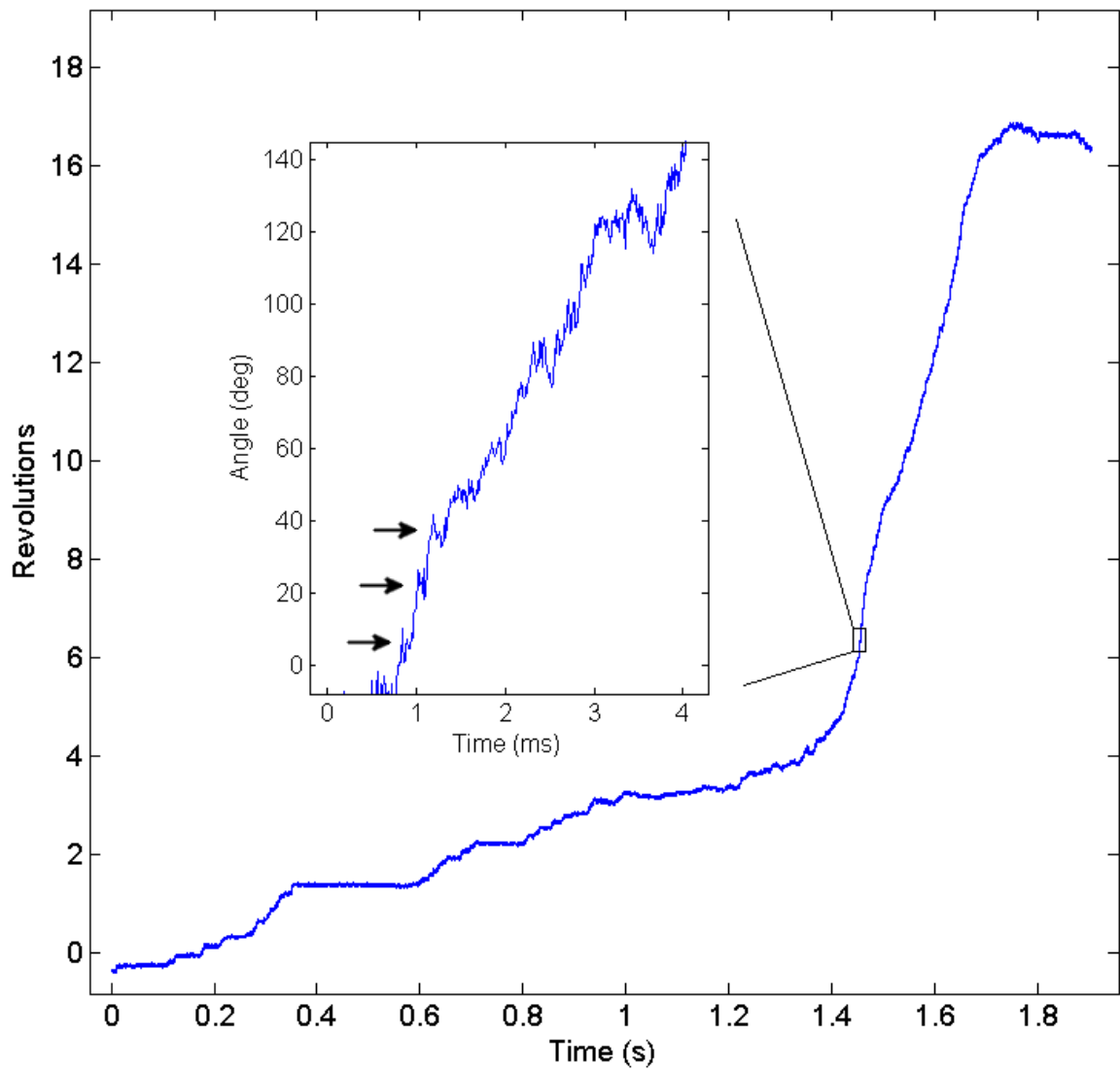
Figure 30: Rotation of a 100 nm streptavidin conjugated gold bead attached to the biotinylated hook in strain MTB24 (*flgE*-BAP-siteC). The rotation starts and stops during the recording over two seconds and is slower (average of 44 Hz in the steep region 1.45 s < t < 1.7 s) than expected (~500 Hz for a 100 nm bead). Stepping rotation was observed (arrows). Step sizes approximately match the 26-fold periodicity found by Sowa *et al.* [18].
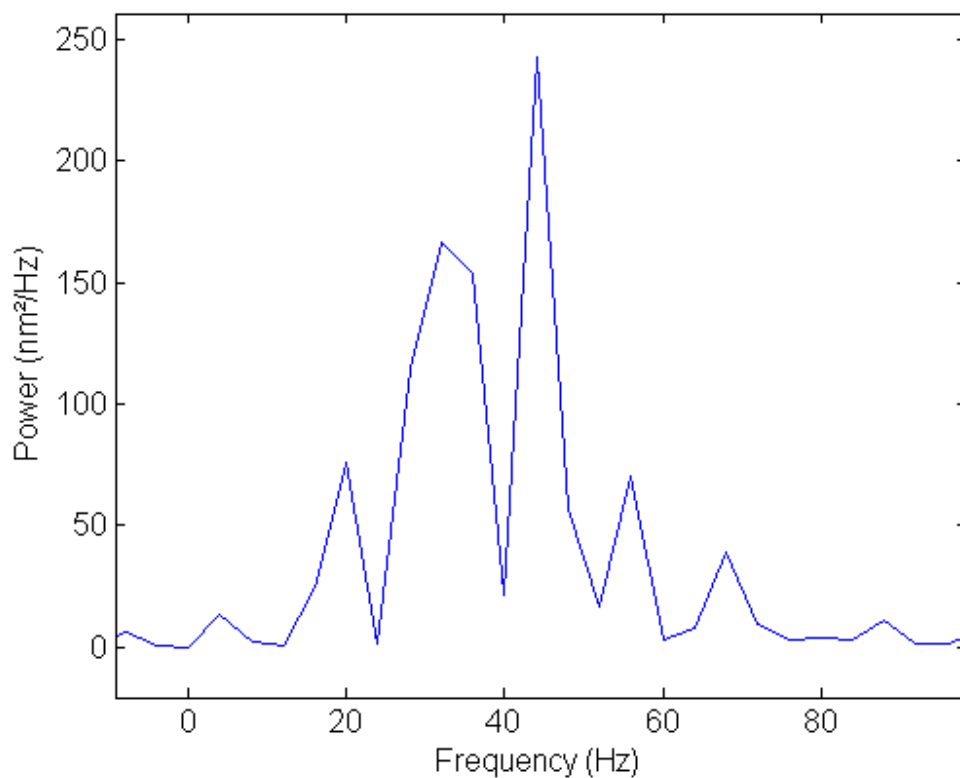
Figure 31: Power spectrum of the interval of fast rotation (1.45 s < t < 1.7). The main peak is at 44 Hz.

Periodicity of the stepping rotation has been analysed in the fast rotating interval (1.45 s < t < 1.7 s) using the empirical characteristic function (ECF) developed by Little *et al.* [43] and a stepping filter, which preferentially fits data with horizontal lines according to a cost function adapted from Kim *et al* [44]. The ECF, similar to the fourier transform, gives a measure of periodicities in the angle density distribution. The result is shown in Figure 32.
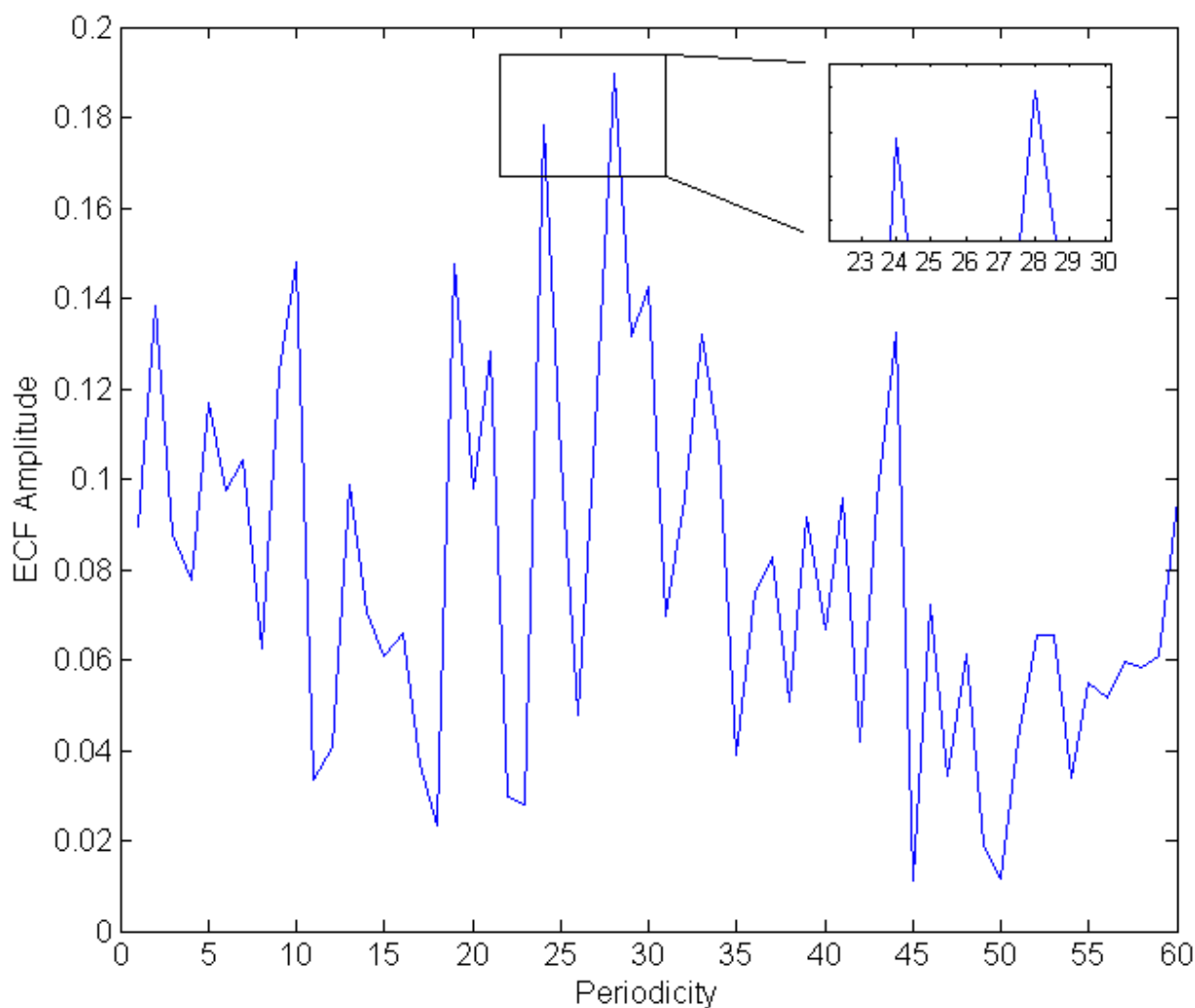
Figure 32: The output of the ECF function. The main periodicities found in the angle density distribution are 24 and 28.

The 24- and 28-fold periodicity found in this analysis differs from the 26 fold periodicity found previously on a setup with higher loads. However the data shown here is based on a single recording of a 12 revolution segment. More experimental data is necessary to analyse stepping periodicity.

Unfortunately experimental results on the dark field setup were not reproducible. Beads were found attached to cells, but not rotating. Various buffers and gold-bead preparations have been tried with no success.

4.5 Hook-compliance

4.5.1 Stereochemistry

As discussed in Section 2.3 the hook is a highly curved structure undergoing continuous rolling rotation during which the protofilaments dynamically change their conformation as well as their repeat distance. An insertion of a 15-mer peptide might affect this natural flexibility and the torsional compliance of the hook. In some cases it might even prevent hook assembly. The effect of the mutations on motility became apparent in the swarm plate assay.
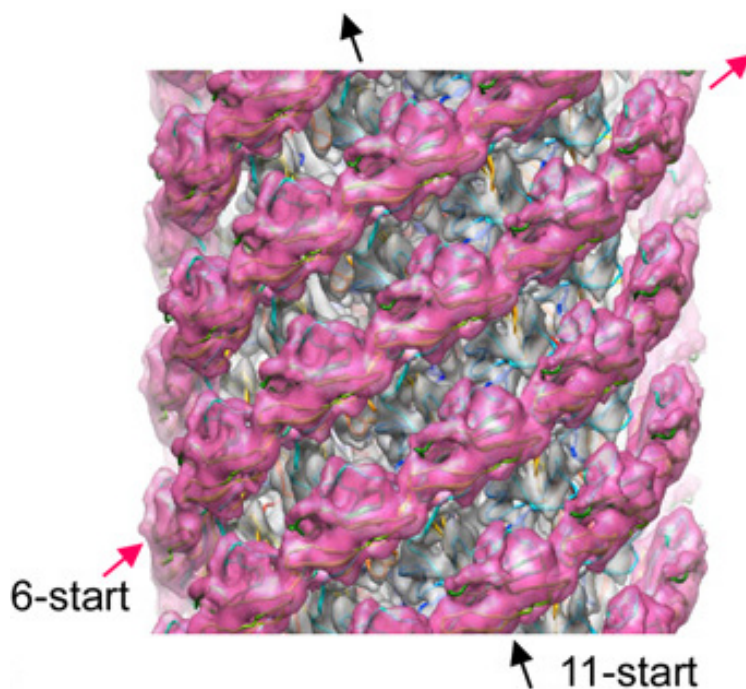
Figure 33: Position of the D2 domains (purple) on the hook structure. The directions of the helical arrays are indicated for the 6-start and 11-start helix. The gap between the protofilaments along the 11-start helix allows the structure to bend, changing the repeat distance on the inner and outer side. (Source: [7])

Binding of free streptavidin to biotin on the hook could have an even greater impact on compliance through steric effects.

The lack of crystal structures of hooks in *flgE*-BAP-mutants prevents modelling of the hook with bound streptavidin. However Figure 34 shows a streptavidin tetramer next to three wildtype FlgE protofilaments to give an idea of the dimensions involved. It seems likely that streptavidin occupation of several neighbouring protofilaments affects the hook's elasticity through steric interaction of neighbouring bound streptavidin entities.
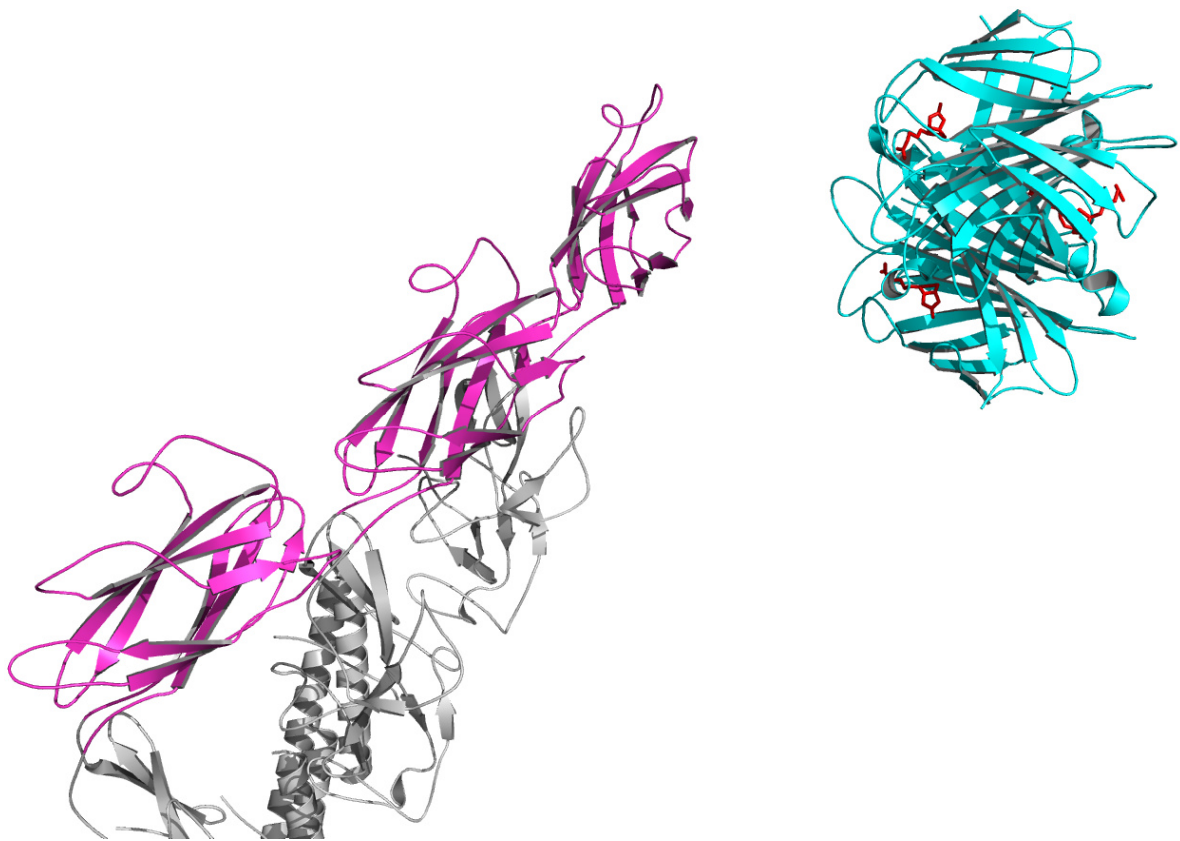
Figure 34: Streptavidin (cyan) with bound biotin (red) next to three FlgE protofilaments (D2 domain purple, other domains grey). (Source: [7], PDB ID: 3A69, 1SWE)

Streptavidin has four binding sites and the repeat distances of the protofilaments along the 11-start helix is variable, ranging from 35 to 59 Å, see Figure 5. The distance of the two bound biotin molecules shown on the left side of the streptavidin tetramer in Figure 34 is about 22 Å. Since this is maximal distance of two bound biotin molecules facing the same way, cross-linking along the 11-start helix of flgE seems unlikely. However it cannot be ruled out, since the distance of two biotin moieties might become even shorter than 35 Å depending on the structure of FlgE with the incorporated BAP.

4.5.2 Preliminary video analysis

It has been assumed but not proven, that the natural flexibility of the hook is necessary for bundle formation in swimming *E.coli*. Visualisation of swimming bacteria and their filaments, in strains engineered for this study, could give insights into the role the hook is playing for bundle formation. Special interest lies on the effect of streptavidin occupation of the biotin sites.

For a preliminary analysis of the effects of streptavidin binding on motility free swimming cells have been observed by light microscopy, see video 2-5 (supplementary material). Motility in MTB9 was compared in normal and streptavidin supplemented (40 µM) Motility Buffer. RP437 served as a wildtype control.

Exposure to streptavidin had no effect on RP437, but severely reduced motility in MTB9 with the majority of the cells seeming to spin or tumble. To further investigate the effect of streptavidin exposure on bundle formation the filaments have to be visualised.

4.5.3 Real time imaging of free swimming bacteria

Filaments are too small to be observed with conventional light microscopes. Turner, *et al.* came up with a simple method to visualise filaments in free swimming bacteria by fluorescently labelling both cell and filaments and observing them in a fluorescence microscope using stroboscopic laser illumination [35]. In this study the epi-fluorescence setup described in 3.3.5.1 is used to observe bundle formation.

The analysis was focused on the strain MTB9, which is clearly motile when not exposed to streptavidin. RP437 was used as a control. Figure 35 and Figure 36 show snapshots of Video 6 – 9 (supplementary material).
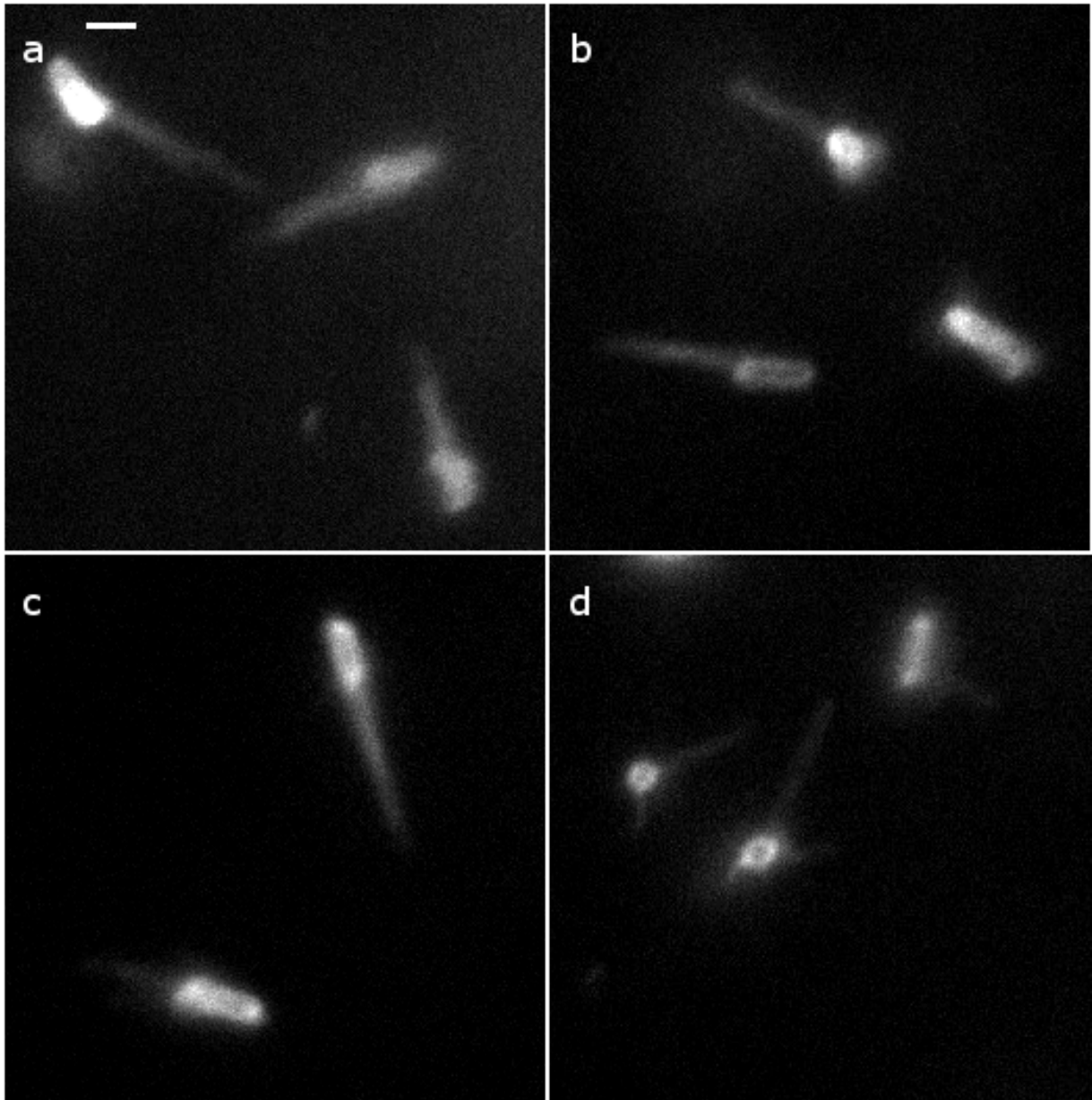
Figure 35: Video snapshots of fluorescently labelled, free swimming bacteria. **a,** RP437 (wildtype control) **b,** RP437 in medium containing streptavidin (20 μM) **c,** MTB9 (*flgE*-BAP-siteC) **d,** MTB9 in medium supplemented with streptavidin (20 μM). Streptavidin only has an effect on MTB9. Individual filaments are sticking out, rather than forming a bundle, resulting in the cell continuously tumbling. Scale bar, 1 μm. Full videos can be found in the supplementary material (Video 6-9).
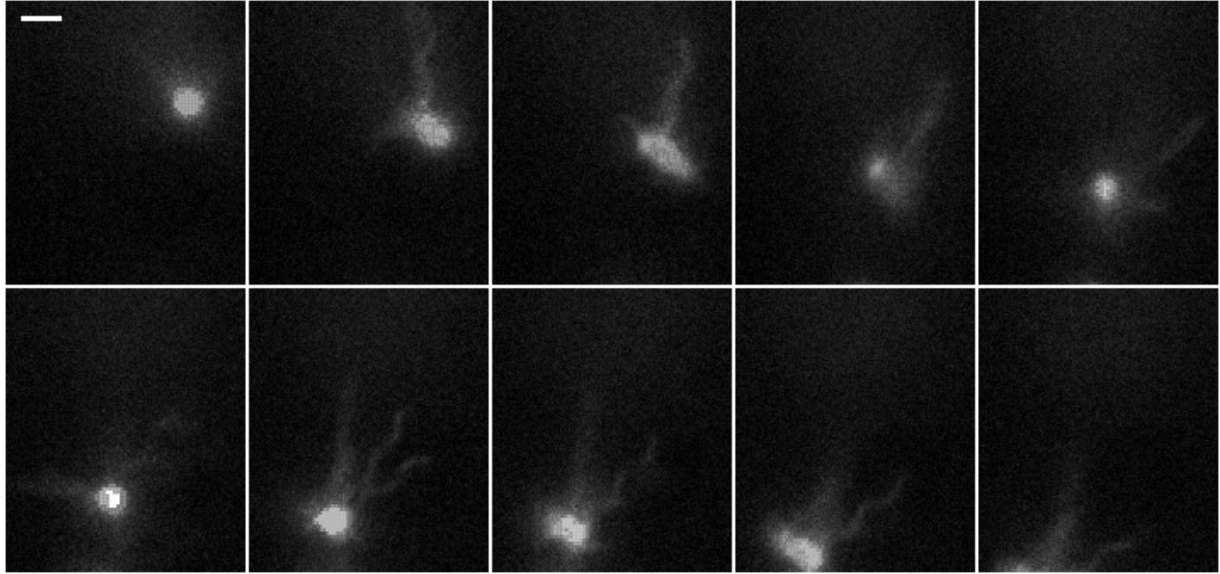
Figure 36: MTB9 (*flgE*-BAP-siteC) in medium supplemented with streptavidin (20 μM) with sequence going from left to right. The cell tumbles continuously not being able to form a flagellar bundle due to streptavidin binding to the biotinylated hook. The sequence is 2.5 seconds long (4 fps). Scale bar, 1 μm. Full video can be found in the supplementary material (Video 9).

4.5.4 Torsional compliance

Video analysis showed the effects of streptavidin binding on the compliance of the hook qualitatively. To quantify this effect the hook's elasticity has to be measured. The tethering assay in the optical trap setup allows measurement of the torsional compliance of the hook, as described in Section 2.8.

The bacterial strain MTB34 was used, which carries the *flgE*-BAP-siteC insertion and a deletion of the gene encoding for the filament protein FliC. The deletion of *fliC* was complemented by vector expression of FliC[st], which allowed attachment of the flagella to the coverslip, due to the sticky filament phenotype. The strain MT02 which is also a sticky filament phenotype served as a wildtype control. Rotating tethered cells were detected by bright-field imaging. The flagellar motors of bacterial cells were locked by flowing in buffer containing 0.1% glutaraldehyde. Block & Berg observed that the measured torsional compliance represents mainly the hook's stiffness if the cells are rotated to up to 150 degrees, after which the stiffer filament contributes as well. As the hook's properties are of interest in this study the cells were rotated to 120-150 degrees in the experiments presented here. Cells were rotated with the optical tweezer and released by shuttering the trapping laser. The rebound on release of the cells was recorded and the angle of the long axis of the bacterium was fitted with an exponential to give the time constant of the rebound, see Figure 37. The long axis was defined by a straight line

passing through the centroid of the cell that minimises the weighted sum of its perpendicular distances to each point on the cell. The frictional drag coefficients were calculated from the dimensions of the cylinder and the viscosity of the medium, which is equivalent to water at room temperature ($\eta_{H_2O} = 10^{-3} \text{Pa s}$). The time constant together with the frictional drag coefficients then allowed calculation of the torsional spring constant.
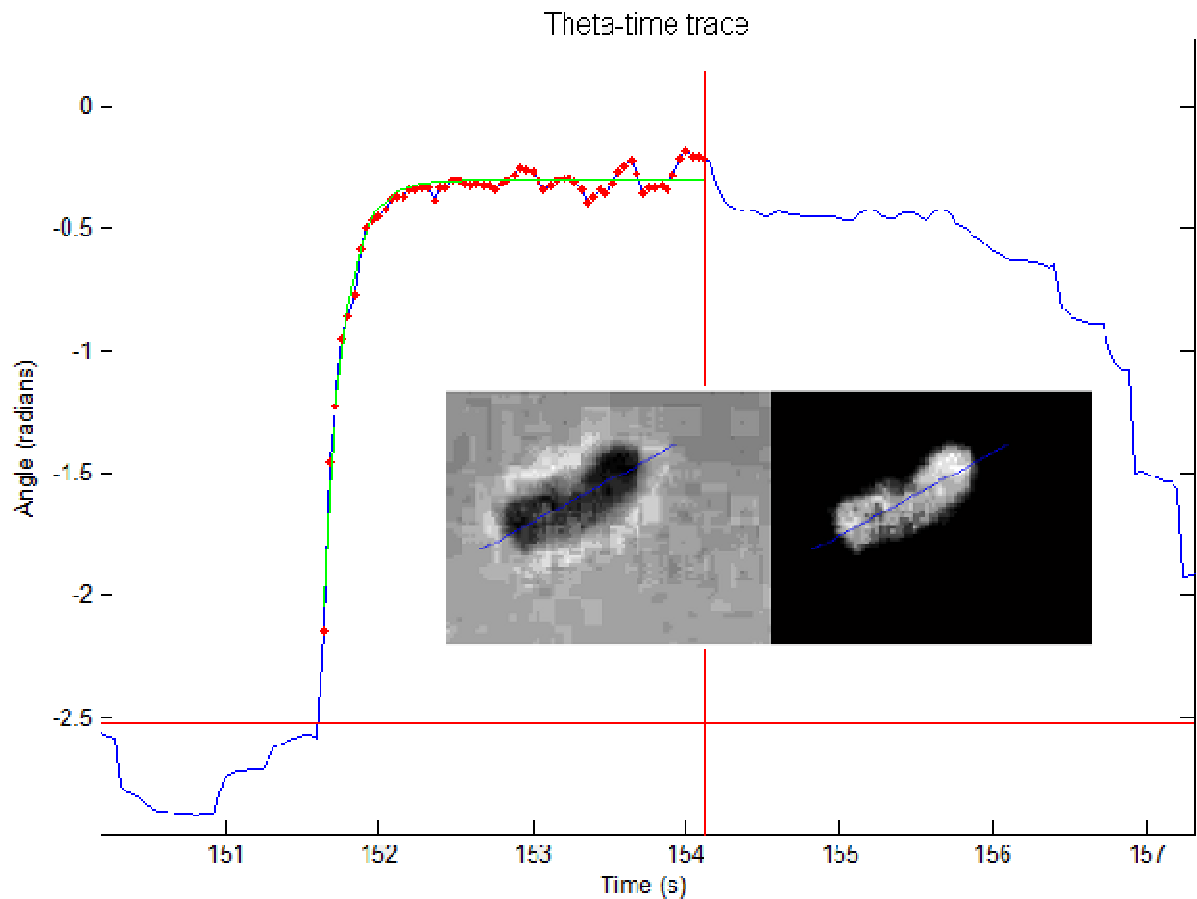
Figure 37: Exponential fit to the angle-time trace of the long axis of the bacterium.

At least 15 rebounds of five cells of each strain were recorded. The torsional spring constants of the individual cells of each strain was computed and averaged. The results are shown in Figure 38. Video 10 (supplementary material) shows a rebound event as recorded on the optical trap setup.
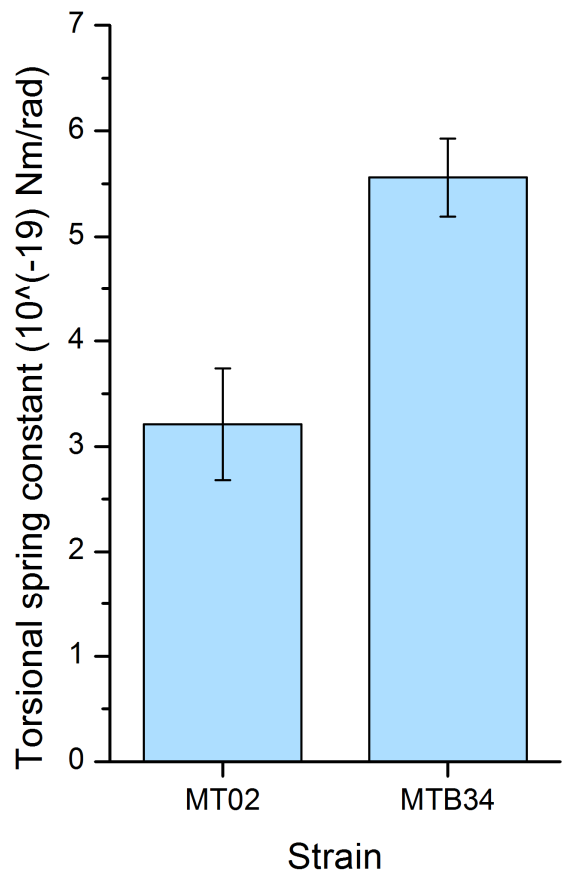
Figure 38: Torsional spring constants. Error bars show the standard error. MT02 is the wildtype control, MTB34 carries the BAP insertion at site C. Preparation of strains included incubation with streptavidin at a concentration of 20 μM.

5 Discussion

The bacterial flagellar hook of *E.coli* was successfully biotinylated by engineering bacterial strains carrying a biotin accepting peptide in the hook-protein FlgE. Two sites were found which support the insertion of the 15-mer biotin accepting peptide, site A (Thr 166 – Val 167) and site C (Ile 221 – Ala 222). Motility remained almost fully intact in *flgE*-BAP-siteC mutants, but was reduced significantly for strains carrying the accepting peptide at site A. The flexibility of the hook is dependent on the continuously changing repeat distances of FlgE protofilaments along the 11-start helix. One possible explanation for the difference in motility is that the insertion at site A is closer to the interface between neighbouring FlgE domains. The additional 15 amino acids in one protofilament could therefore easily affect the next protofilament through steric interaction.

Stepping rotation was observed in the dark field setup, yielding step sizes approximately matching the 26-fold periodicity found by Sowa *et al* [18]. However this analysis was based on a single cell recording since attachment of beads was not reproducible with the procedures used in this study. Possible reasons for the low yields of attachment include the interaction of streptavidin with the cell-surface resulting in non-specific binding or prevention of rotation. Further possible reasons are low accessibility of the biotin moieties for streptavidin-covered beads and occupation of the biotin sites by binding of residual free streptavidin.

One way to optimise the preparation of streptavidin-conjugated gold beads could be to reduce non-specific interaction with the cell-surface by pegylating the beads. Attachment yields could also be improved by using biotin-coated gold beads with biotinylated hooks where the biotin-sites are already occupied by free streptavidin. Since two binding sites of a bound streptavidin are still facing outwards they could be more easily accessible than the biotinylated sites themselves.

Effects of streptavidin binding on bundling formation was observed in fluorescently labelled free-swimming cells carrying the BAP at site C. Bound streptavidin clearly prevented the cells' flagella from bundling, impairing their motility. These findings proved that the flexibility of the hook is necessary for bundle formation.

Using optical tweezers on tethered cells allowed further analysis of the elastic properties of the hook and comparison between wildtype and engineered strains with bound streptavidin. The torsional spring constant of the strain carrying the insertion at site C was shown to be significantly higher than the value obtained for wildtype hooks.

6 Outlook

With the biotinylated hook a tool with various applications was created.

With further optimisation of the current protocols the biotinylated hook could be used for improved attachment of gold beads for measurement of stepping rotation using dark field microscopy.

The measurement of the torsional compliance and the free-swimming analysis showed that the engineered strains provide a tool for stiffening the bacterial hook. A stiffer hook could provide a more direct link to the motor in the gold bead assay. Further analysis of the different components of the hook's elasticity could give insights into hook-dynamics. Preliminary analysis suggested that there might be several domains of torsional compliance in the hook.

The engineered strains also provide an easy way to mark the position of the flagellar motors on bacterial cells, which for example has applications for investigating bacterial growth and cell shape.

Furthermore the entire flagellum with the biotinylated hook provides a building block for synthetic biology with promising applications such as creating artificial swimmers by attaching the flagella with biotinylated hooks to the small rotational motor F_1F_o ATP synthase.

7 Appendices

Appendix A: Buffers and solutions

Motility Buffer (for strains with wildtype stators)

Potassium phosphate	10 mM
EDTA	0.1 mM
pH 7.0	

Motility Buffer (for chimeric strains)

Potassium phosphate	10 mM
NaCl	83 mM
EDTA	0.1 mM
pH 7.0	

Luria-Bertani-broth

Bacto-tryptone	10 g/l
Yeast extract	5 g/l
NaCl	5 g/l
pH 7.0	

Tryptone-broth

Bacto-tryptone	10 g/l
NaCl	5 g/l
pH 7.0	

LB-agar

Bacto-tryptone	10 g/l
Yeast extract	5 g/l
NaCl	5 g/l
Agar	20 g/l
pH 7.0	

Sucrose medium

Bacto-tryptone	10 g/l
Yeast extract	5 g/l
Sucrose	100 g/l
pH 7.0	

Appendix B: Primer sequences

flgE primers

Name	Sequence	Restriction site	Use
flgE_A	TACA<u>CCATGG</u>CCTTTTCTCAAGCG	NcoI	flgE into pQE60
flgE _D	ATCG<u>GGATCC</u>TTAGCGTAAGTTAACCAG	BamHI	
flgE_SbfI_F	CGGC<u>CCTGCAGG</u>ATGGCCTTTTCTCAAGCG	SbfI	flgE_sites from pQE60 into pDS132
flgE_SacI_R	GCCG<u>GAGCTC</u>TTAGCGTAAGTTAACCAG	SacI	
FlgE_BAP_test_Fwd2	CAACCTGAATTCCAGTGATCC	-	Used as a PCR screen for BAP strains (263bp without BAP, 308bp with)
FlgE_BAP_test _Rev2	TATTCGCCATCGCACCATCC	-	
FlgE_seq_Fwd	GGTGTGATCCGCGGCAACAG		FlgE primers dedicated for sequencing
FlgE_seq_Rev	CCTGTTGATTCAGTGTCTGG		

fliC primers

Name	Sequence	Restriction site	Use
fliC_up_F	GCCG<u>GAGCTC</u>CTGCTGGTGGTGCTGGTG	SacI	Making delta fliC PDS132 construct
fliC_up_R	CGCC<u>TCTAGA</u>CATGATTCGTTATCCTATATTG	XbaI	
fliC_down_F	GCGC<u>TCTAGA</u>TAATCGTTGTAACCTGATTAAC	XbaI	
fliC_down_R	GTCGAA<u>CCTGCAGG</u>CGCAATGC	SbfI	
FliC_ seq_Fwd	CCAGATGGGTGACGCTGATG		Used as a PCR screen for fliC deletion (2603bp with fliC; 1118bp without)
FliC_ seq_Rev	CTGCGTAAGTTGTAAATGCC		

8 References

[1] M. A. B. Baker and R. M. Berry, "An introduction to the physics of the bacterial flagellar motor: a nanoscale rotary electric motor," *Contemporary Physics*, vol. 50, no. 6, pp. 617-632, Nov. 2009.

[2] R. D. Astumian, "Design principles for Brownian molecular machines: how to swim in molasses and walk in a hurricane," *Physical Chemistry Chemical Physics*, vol. 9, no. 37, pp. 5067-5083, Oct. 2007.

[3] H. C. Berg, "Bacterial flagellar motor," *Current Biology*, vol. 18, pp. 689-691, 2008.

[4] D. Thomas, D. G. Morgan, and D. J. DeRosier, "Structures of the bacterial flagellar motors from two FliF-FliG gene fusion mutants," *Journal of Bacteriology*, vol. 183, pp. 6404-6412, 2001.

[5] E. Katayama, T. Shiraishi, K. Oosawa, N. Baba, and S. Aizawa, "Geometry of the flagellar motor in the cytoplasmic membrane of Salmonella typhimurium as determined by stereo-photogrammetry of quick-freeze deep-etch replica images.," *Journal of Molecular Biology*, vol. 255, pp. 458-475, 1996.

[6] T. Minamino and K. Namba, "Self-Assembly and Type III Protein Export of the Bacterial Flagellum," *Journal of Molecular Microbiology and Biotechnology*, vol. 7, pp. 5-17, 2004.

[7] T. Fujii, T. Kato, and K. Namba, "Specific Arrangement of a-Helical Coiled Coils in the Core Domain of the Bacterial Flagellar Hook for the Universal Joint Function," *Structure*, vol. 17, pp. 1-9, Nov. 2009.

[8] F. A. Samatey and K. Namba, "Structure of the bacterial flagellar hook and implication for the molecular universal joint mechanism," *Nature*, vol. 431, pp. 1062-1068, Oct. 2004.

[9] T. Saito, et al., "Flagellar filament elongation can be impaired by mutations in the hook protein FlgE of Salmonella typhimurium: a possible role of the hook as a passage for the anti-sigma factor FlgM," *Molecular Microbiology*, vol. 27, no. 6, pp.

1129-1139, 1998.

[10] S. M. Block, D. F. Blair, and H. C. Berg, "Compliance of bacterial flagella measured with optical tweezers," *Nature*, vol. 338, pp. 514-518, Apr. 1989.

[11] S. G. Taylor, "Film Notes for Low-Reynolds-Number Flow," National Committee for Fluid Mechanics Films, 1967.

[12] P. Nelson, *Biological Physics: Energy, Information, Life*. W.H. Freeman and Company, 2003.

[13] M. Kim, J. C. Bird, A. J. Van Parys, K. S. Breuer, and T. R. Powers, "A macroscopic scale model of bacterial flagellar bundling," *Proceedings of the National Academy of Sciences*, vol. 100, no. 26, pp. 15481-15485, Dec. 2003.

[14] J. Xing, F. Bai, R. Berry, and G. Oster, "Torque-speed relationship of the bacterial flagellar motor," *Proceedings of the National Academy of Sciences USA*, vol. 103, pp. 1260-1265, 2006.

[15] M. Silverman and M. Simon, "Flagellar rotation and the mechanism of bacterial motility," *Nature*, vol. 249, pp. 73-74, May 1974.

[16] X. Nan, P. A. Sims, and X. Sunney Xie, "Organelle Tracking in a Living Cell with Microsecond Time Resolution and Nanometer Spatial Precision," *ChemPhysChem*, vol. 9, pp. 707-712, 2008.

[17] H. C. Berg, "Does the flagellar rotary motor step?," *Cell Motility*, pp. 47-56, 1976.

[18] Y. Sowa, et al., "Direct observation of steps in rotation of the bacterial flagellar motor," *Nature*, vol. 437, pp. 916-919, 2005.

[19] S. M. Block, B. D. F, and B. H. C, "Compliance of bacterial flagella measured with optical tweezers," *Nature*, vol. 338, pp. 514-517, Apr. 1989.

[20] M. Tirado and J. G. de la Torre, "Translational friction coefficients of rigid, symmetric top macromolecules. Application to circular cylinders," *J. Chem. Phys.*, vol. 71, no. 6, pp. 2581-2587, Sep. 1979.

[21] M. Tirado and J. G. de la Torre, "Rotational dynamics of rigid, symmetric top macromolecules. Application to circular cylinders.," *J. Chem. Phys.*, vol. 73, no. 4, pp.

1986-1993, 1980.

[22] J. Happel and H. Brenner, *Low Reynolds number hydrodynamics*. The Hague: Martinus Nijhoff Publishers, 1983.

[23] N. M. Green, "Avidin," *Advances in Protein Chemistry*, vol. 29, pp. 85-133, 1975.

[24] D. Beckett, E. Kovaleva, and P. Schatz, "A minimal peptide substrate in biotin holoenzyme synthetase-catalyzed biotinylation," *Protein Science*, vol. 8, pp. 921-929, 1999.

[25] M. Howarth and A. Y. Ting, "Imaging proteins in live mammalian cells with biotin ligase and monovalent streptavidin," *Nature Protocols*, vol. 3, no. 3, pp. 534-545, Mar. 2008.

[26] A. Haldimann and B. Wanner, "Conditional replication, integration, excision, and retrieval plasmid-host systems for gene structure-function studies of bacteria.," *Journal of Bacteriology*, vol. 183, pp. 6384-6393, 2001.

[27] B. Scharf, K. Fahrner, L. Turner, and H. Berg, "Control of direction of flagellar rotation in bacterial chemotaxis," *Cell Biology*, vol. 95, pp. 201-206, Jan. 1998.

[28] J. S. Parkinson, "Complementation Analysis and Deletion Mapping of Escherichia coli Mutants Defective in Chemotaxis," *Journal of Bacteriology*, vol. 135, no. 1, pp. 45-53, Jul. 1978.

[29] T. Baba, et al., "Construction of Escherichia coli K-12 in-frame, single-gene knockout mutants: the Keio collection," *Molecular Systems Biology*, Feb. 2006, doi:10.1038/msb4100050.

[30] N. Philippe, J.-P. Alcaraz, E. Coursange, J. Geiselmann, and D. Schneider, "Improvement of pCVD442, a suicide plasmid for gene allele exchange in bacteria," *Plasmid*, vol. 51, pp. 246-255, 2004.

[31] D. F. Blair and H. C. Berg, "Restoration of torque in defective flagellar motors," *Science*, vol. 242, pp. 1678-81, 1988.

[32] J. Sambrook and T. Maniatis, *Molecular Cloning: A Laboratory Manual.* Cold Spring Harbor Laboratory Press, 1989.

[33] P. Gay, D. Le Coq, M. Steinmetz, E. Ferrari, and J. Hoch, "Positive Selection Procedure for Entrapment of Insertion Sequence Elements in Gram-Negative Bacteria," *Journal of Bacteriology*, vol. 153, no. 3, pp. 1424-1431, Mar. 1983.

[34] N. C. Darnton, L. Turner, S. Rojevsky, and H. C. Berg, "On Torque and Tumbling in Swimming Escherichia coli," *Journal of Bacteriology*, vol. 189, pp. 1756-1764, Mar. 2007.

[35] L. Turner, W. S. Ryu, and H. C. Berg, "Real-Time Imaging of Fluorescent Flagellar Filaments," *Journal of Bacteriology*, vol. 182, no. 10, pp. 2793-2801, May 2000.

[36] R. Yasuda, H. Noji, M. Yoshida, K. Kinosita, and H. Itoh, "Resolution of distinct rotational substeps by submillisecond kinetic analysis of F1-ATPase," *Nature*, vol. 410, pp. 898-904, 2001.

[37] S. Furuike, et al., "Temperature Dependence of the Rotation and Hydrolysis Activities of F1-ATPase," *Biophysical Journal*, vol. 95, pp. 761-770, Jul. 2008.

[38] T. Pilizota, "A programmable optical angle clamp for rotary molecular motors," University of Oxford Dphil thesis, 2006.

[39] I. Bates, et al., "Membrane Lateral Diffusion and Capture of CFTR within Transient Confinement Zones," *Biophysical Journal*, vol. 91, pp. 1046-1058, Aug. 2006.

[40] G. Digby, P. Sethi, and N. Lambert, "Differential dissociation of G protein heterotrimers," *Journal of Physiology*, vol. 586, no. 14, pp. 3325-3335, 2008.

[41] L. Oddershede, J. Dreyer, S. Grego, S. Brown, and K. Berg-Sørensen, "The Motion of a Single Molecule, the λ-Receptor, in the Bacterial Outer Membrane," *Biophysical Journal*, vol. 83, pp. 3152-3161, Dec. 2002.

[42] T. Shaikh, et al., "A partial atomic structure for the flagellar hook of Salmonella typhimurium," *Proceedings of the National Academy of Sciences*, vol. 102, pp. 1023-1028, Jan. 2005.

[43] M. A. Little, et al., "Steps and bumps: precision extraction of discrete states of molecular machines using physically-based, high-throughput time series analysis", Under review.

[44] S. J. Kim, K. K. S. Body, and G. D, "$\ell 1$ trend filtering," *SIAM review*, 2009.

[45] H. C. Berg and R. A. Anderson, "Bacteria swim by rotating their flagellar filaments," *Nature*, vol. 245, pp. 380-392, Oct. 1973.

[46] S. Kojima and D. Blair, "Conformational change in the stator of the bacterial flagellar motor," *Biochemistry*, vol. 40, pp. 13041-13050, 2001.

[47] S. M. Block, D. F. Blair, and H. C. Berg, "Compliance of Bacterial Polyhooks Measured with Optical Tweezers," *Cytometry*, vol. 12, pp. 492-496, 1991.

[48] R. M. Berry, "Theories of rotary motors," *Philosophical Transactions of the Royal Society of London. Series B, Biological Sciences*, vol. 355, pp. 503-509, 2000.

[49] Y. Asai, T. Yakushi, I. Kawagishi, and M. Homma, "Ioncoupling determinants of Na+-driven and H+-driven flagellar motors," *Journal of Molecular Biology*, vol. 327, pp. 453-463, 2003.

9 List of Figures

Acknowledgements

I would like to express my gratitude to the following people

- Prof Philip Tinnefeld for his supervision and advice and for giving me the opportunity to work on this project.
- Dr Richard Berry for offering me a position in his lab and for his continuous support throughout the project.
- Dr Mostyn Brown for introducing me to the methods in molecular biology, his supervision and assistance.
- Dr Bradley Steel for his helpful advice.
- Everyone in the Oxford Molecular Motors group for their continuous help.
- Prof Judy Armitage and her group for welcoming me in their laboratory and helping me with my project.

Special thanks to my parents for being incredibly supportive throughout my education.

Finally I would like to thank Viola for encouraging me in my decision to take on this project and for being there for me.

Erklärung

Hiermit erkläre ich, die vorliegende Arbeit selbständig und ausschließlich unter Verwendung der angegebenen Quellen und Hilfsmittel angefertigt zu haben.

München, den 30. September 2010

Claudio Silvestrin